










Lateral Evolution of the Deep Crustal Structure of the Lesser Antilles Subduction Zone from Wide-Angle Seismic Modeling

Frauke Klingelhofer ^{*1}, Boris Marcaillou ², Muriel Laurencin ³, Mireille Laigle ², Jean-Frédéric Lebrun ³, Laure Schenini ², David Graindorge ¹, Mikael Evain ¹, Heidrun Kopp ^{4,5}

¹Geo-Ocean, UMR6538 Univ Brest, CNRS, Ifremer, UBS, France | ²Geoazur, Université Côte d'Azur, CNRS, IRD, Observatoire de la Côte d'Azur, Nice, France | ³UMR5243 Geosciences Montpellier, Antilles University, CNRS, Montpellier University, Pointe-à-Pitre, France | ⁴GEOMAR, Kiel, Germany | ⁵Christian-Albrechts University, Kiel, Germany

Abstract The Lesser Antilles is a subduction zone where devastating earthquakes occur with a long recurrence interval. Here, oceanic lithosphere from the Mid-Atlantic spreading center subducts at a slow convergence velocity of 20 mm/yr underneath the Caribbean Plate. Offshore Antigua and Barbuda previous work proposed the existence of a patch of amagmatically accreted oceanic crust bearing a high percentage of serpentinite and therefore a high fluid content. During the ANTITHESIS cruise a seismic profile was acquired in this zone of relative seismic quiescence. The combined wide-angle and reflection seismic profile was recorded using 25 ocean-bottom seismometers, a 126 l (7699 cu. in.) tuned airgun array and a 2.8 km long seismic streamer. The resulting velocity model images the forearc and oceanic crust to a depth of 30 km. The oceanic crust is only about 5 km thick and was best modelled as one single layer with a constant velocity gradient. Gravity modelling indicates that the oceanic crustal densities are lower than magmatic rock densities, thus in good agreement with the presence of relatively light serpentinised mantle material incorporated in the crust. The fluids leaving this highly hydrated subducting slab at different depths might be responsible for the subdued seismicity of the study region. The forearc is about 25 km thick and has velocities slightly higher than continental crust. Along the forearc the crustal thickness is highly variable between 15 and 30 km.

Executive Editor:
J. Kim Welford
Associate Editor:
Jack Williams
Technical Editor:
Roxana Stanca

Reviewers:
Anonymous
Reviewer 1
Anonymous
Reviewer 2

Submitted:
12 February 2024
Accepted:
7 July 2025
Published:
13 October 2025

Plain language summary In the Lesser Antilles an oceanic plate of the Atlantic moves underneath the Caribbean plate. This process creates frequent earthquakes at the contact between the two plates. Seismicity of the region of the past 50-years long instrumental period is not distributed regularly but is divided into regions of higher seismicity and local gaps. One of these gaps is located offshore Antigua and Barbuda, where earlier work proposed that the downgoing crust has an unusually high water content. These fluids will return to the seafloor and might be responsible for the lack of earthquakes. Our project included the acquisition of a seismic profile, using airguns generating strong acoustic signals and seismometers deployed on the seafloor. The resulting velocity model shows the crustal structures to a depth of up to 30 km. This model indicates that the downgoing crust indeed is unusual and might carry a large amount of water controlling the seismicity of the region.

1 Introduction

Most of the seismic energy of the Earth is released in subduction zones, posing a substantial hazard potential. Several factors have been proposed to influence the seismicity of subduction zones, e.g. the age of the subducting plate (e.g. *Ruff and Kanamori*, 1980), the spatial and temporal variations of the interplate seismic coupling (e.g. *Mccaffrey*, 2008), barriers and asperities along the plate interface (e.g. *Cloos and Shreve*, 1996; *Scholz and Small*, 1997; *Wang and Bilek*,

2011), temperature along the interplate contact (e.g. *Hyndman and Wang*, 1993), incoming sediment thickness and compaction (e.g. *Tsuru et al.*, 2002), deformation of the overriding plate (e.g. *Collot et al.*, 2004) as well as fluid overpressure along the interplate megathrust (e.g. *Wallace et al.*, 2012), and nature of subducted material (*Barnes et al.*, 2020). In order to evaluate these aspects, a good knowledge of the crustal structure of the forearc and the downgoing plate is a prerequisite.

Subduction zones are also relevant for the formation of new continental crust, which has been proposed to form by magmatic processes in the volcanic arcs of subduction

*✉ fklingel@ifremer.fr

zones (e.g. *Taylor, 1967; Jagoutz and Kelemen, 2015*). To explain the formation of continental crust from basaltic melts, delamination of the lower ultramafic layer has been suggested (e.g. *Kay and Kay, 1993*). Numerical modelling indicates that the volume of newly formed crust might depend on the age of the subducted slab (*Nikolaeva et al., 2008*). A 3-layer arc crust with a high velocity ($> 6.5\text{--}7.5\text{ km/s}$) and dense ($\sim 2,85\text{ g/cm}^3$) lower crustal unit, probably mafic, has been identified in the Lesser Antilles (e.g. *Westbrook et al., 1988*). Its lateral extent, thickness variation, and origin have yet to be investigated.

Despite large devastating historical earthquakes (e.g. the Mw 7-7.5 Martinique and Mw 8-8.5 Guadeloupe earthquakes in 1839 and 1843 (*Bernard and Lambert, 1988; Feuillet et al., 2011; Hough, 2013*)), modern day seismicity is moderate to slightly elevated (Mw < 6) in the Lesser Antilles subduction zone (e.g. *Gonzalez et al. (2018); Bie et al. (2019)* and references therein), where the western central and equatorial Atlantic oceanic lithosphere is subducting underneath the Caribbean plate at a slow rate of 20 mm/yr in a N254° direction (*DeMets et al., 2000*) (Figure 1). A lack of frequent inter-plate thrust events also characterizes the Lesser Antilles subduction zone (*Gonzalez et al., 2018*). Geodetic measurements reveal only very moderate strain accumulation along the plate interface (*Symithe et al., 2015; van Rijnsingen et al., 2020*). Recent tomographic results demonstrated a great variability of velocity anomalies within the Lesser Antilles, all interpreted as due to large volumes of fluid released during subduction from the highly fractured subducting equatorial Atlantic Ocean lithosphere (*Laigle et al., 2013a; Paulatto et al., 2017; Schlaphorst et al., 2016; Bie et al., 2022a*). However, part of the margin north of 17°N remains less intensively studied. There, north of the Fifteen-Twenty-fracture zone, subducts the Cretaceous-Central Atlantic oceanic lithosphere. This part of the Northern Lesser Antilles margin (Figure 1) presents a significantly reduced seismic activity (*Massin et al., 2021*). *Marcaillou et al. (2021)* discovered that the oceanic crust close to the trench was accreted along an amagmatic segment at the Mid-Atlantic Ridge, thus likely hosting a large amount of serpentinite. In this region, the seafloor is characterized by the presence of numerous mud-volcanoes and other fluid expulsion features (Figure 2). This vigorous fluid flow also influences heat flow at the seafloor (Figure 1 and *Ezenwaka et al., 2022*). In our study region, offshore of Saint Martin Island, downward percolation of cold fluids through crustal faults at the trench is at the origin of hydrothermal cooling at the trench and below the accretionary prism, whereas warm fluid migration from depth through fault zones in the forearc generates hydrothermal warming there (*Ezenwaka et al., 2022*). Offshore Martinique, in the Central Lesser Antilles, heat flow anomalies are explained by warm fluids released at depths migrating towards the seafloor along the subduction interface producing hydrothermal warming at the trench (*Ezenwaka et al., 2022*).

The main objective of this study was to resolve seismic velocities in a region where reflection seismic data imaged high amplitude reflectors dipping towards the Mid-Atlantic Ridge in the Lesser Antilles. Although published reflection seismic data (*Marcaillou et al., 2021*) constrain well the geometry of the subduction here, wide-angle seismic data bring additional information about the nature of the crust. Although other profiles exist (*Laurencin et al., 2018*), the profile we present is as yet the only profile located in this region of unusual oceanic basement. It has been acquired in the Northern Lesser Antilles, to the north-west of Barbuda Island, along the 200-km-long wide-angle and reflection seismic line AN06 spanning from the trench to the inner forearc. We investigate wide-angle-derived velocity variations in the downgoing and overriding plates together with multi-channel seismic (MCS) data interpretations and gravity models in order to shed light on the deep structure of the Lesser Antilles subduction zone. This profile is located in a region of pervasive detachment faults in the lower plate at and near the trench, interpreted to originate from the slow spreading Mid-Atlantic Ridge and reactivated close to the trench by the subduction (*Marcaillou et al., 2021*). However, the unique contribution from wide-angle seismic data is the calculation of seismic velocities which can be used to constrain the lithology of the different layers in the subsurface. So, this study was carried out to determine the geometry of the subduction zone offshore Barbuda and Antigua, to resolve the nature of the downgoing slab showing the detachment faults, and to address the crustal properties along the forearc of the Northern Lesser Antilles margin from the Karukera Spur to the Virgin Islands (Figure 1). A second objective is the comparison of the structures found along this profile to other wide-angle seismic profiles and to observe variability of the structures in the forearc.

2 Regional context and past work

Early deep sounding seismic work on the crustal structure of the Lesser Antilles margin mainly focused on the margin south of 17°N, imaging the internal structure of the Barbados accretionary wedge and the crustal structure across the Antilles Arc and Aves Ridge (*Westbrook et al., 1988*). More recently, wide-angle and reflection seismic data acquired between 15°N and 17°30'N provided a P-wave velocity model down to 15 km depth, which images two distinct forearcs (*Bangs et al., 2003; Christeson et al., 2003; Laigle et al., 2013b; Evain et al., 2013*). The outer forearc presents a thinned and deformed crustal layer that acts as a soft backstop to the accretionary prism. The inner forearc crust is up to 25 km thick. The inner forearc crust rises to shallow depth at the Karukera Spur, and crops out at its northern tip in La Désirade Island, where Late Jurassic to Early Cretaceous plutonic and effusive magmatic rocks are exposed (*Neill et al., 2010; Lardeaux et al., 2013* and references therein). Two wide-angle seismic models south and north of the Guadeloupe Island extend from the forearc to the back arc, the TRAIL P2 profile (*Kopp et al., 2011*) and the GA03 profile (*Padron et al., 2021*).

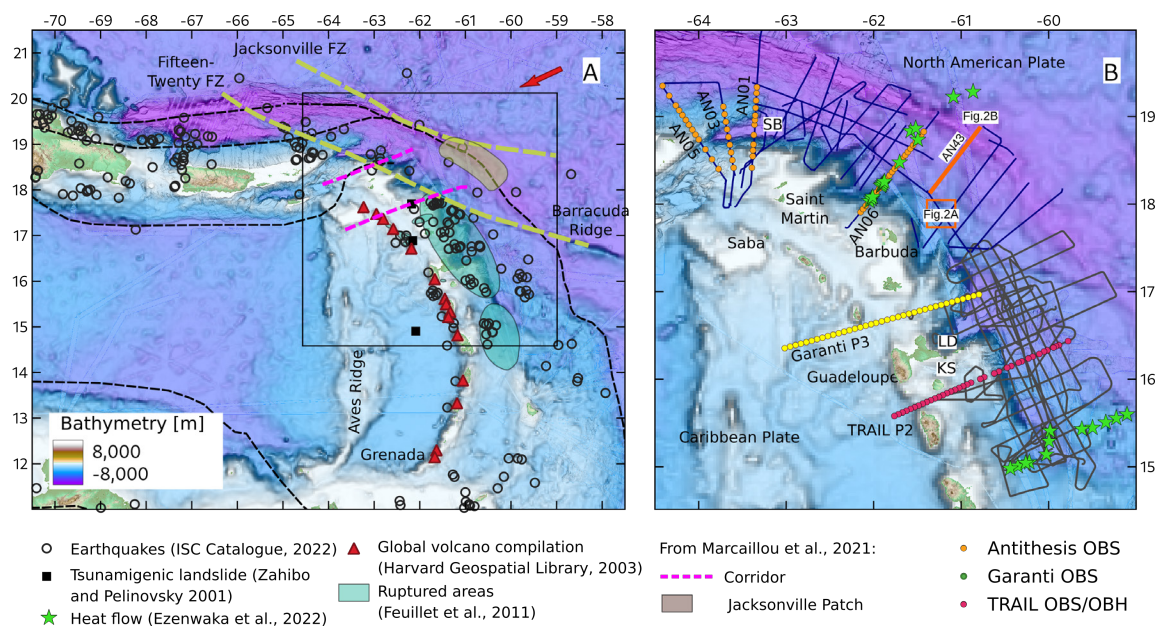


Figure 1 – (A) Tectonics and seismicity of the study region. **(B)** Location of reflection and wide-angle seismic profiles from previous oceanographic studies and the ANTITHESIS cruise (blue and grey lines). FZ = Fracture zone, KS = Karukera Spur, SB = Sombrero Basin, LD = La Désirade. Red arrow: relative NAM/CAR plate motion at 20 km/Ma. Orange box shows location of Figure 2A and orange line location of Figure 2B. Pink dashed lines delimit the zone of reduced seismicity from Marcaillou et al. (2021). Additional data sources: Zahibo and Pelinovsky (2001); Harvard Geospatial Library (2003); Feuillet et al. (2011); Ezenwaka et al. (2022); International Seismological Centre (2022).

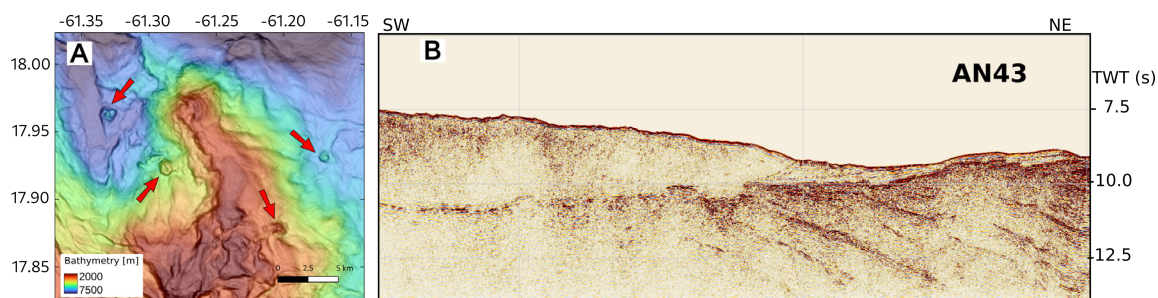


Figure 2 – (A) Seafloor bathymetry of the study region showing four mud-volcano structures in an area of 15x15 km. **(B)** Part of seismic profile AN43 showing high amplitude deep reflectors in the downgoing oceanic crust. Location of A and B is shown in Figure 1.

Both profiles image a 24-km-thick typical 3-layer arc crust with little thickness variation from the back arc to the forearc. More results from these two profiles will be discussed below. The two profiles do not extend to the deformation front and only the TRAIL P2 profile images the subducted plate that presents a classic oceanic crust velocity structure and thickness (Kopp et al., 2011).

North of 18°N, the Northern Lesser Antilles subduction zone segment was poorly investigated despite a debated origin for its very low seismic activity. During the ANTITHESIS cruises (Marcaillou and Klingelhofer, 2013), combined bathymetry, wide-angle (WAS) and multi-channel (MCS) seismic data as well as heat-flow measurements were acquired to investigate the shallow to deep structure and the thermal regime of the Northern Lesser Antilles subduction zone from 17°30' to 19°N. Here, the slab is steeply inclined to the south and shallowing towards the north particularly north of the Sombrero Basin that separates the Northern Lesser Antilles (NLA) from the Virgin Island forearc. This shallower location might induce a stronger coupling

of the subduction towards the north and offer an explanation for the higher seismicity at the Virgin Islands forearc (Laurencin et al., 2018, 2019). A recent wide-angle seismic experiment explored the oceanic crust south of the Barracuda Ridge and before its subduction (Allen et al., 2019; Davy et al., 2020). The two profiles located 300 km apart imaged a strong spatial segmentation of the crust with tectonically and magmatically dominated segments in about equal proportions.

Further information about the deep structure of the Lesser Antilles has been gained through receiver function analysis, S-wave dispersion, and seismic tomography (Schlaphorst et al., 2016; Paulatto et al., 2017; Gonzalez et al., 2018; Melekhova et al., 2019; Bie et al., 2022a). The depth of the slab is generally greater in the north offshore Guadeloupe and shallowing to the south towards Grenada as well as to the north towards Saba. A strong mid-crustal reflector was modeled from receiver functions at around 10-25 km depth. Seismic tomography using active and passive seismic data maps

the multistage dehydration of the slab and its lateral variations in the Lesser Antilles region in relation with serpentinized peridotite exhumed at slow-spreading crust of the Mid-Atlantic Ridge near the Fifteen-Twenty and Marathon fracture zones.

3 Data acquisition, quality, and initial processing

During the ANTITHESIS 1 cruise (Marcaillou and Klingelhofer, 2013) four combined wide-angle and reflection seismic lines were acquired in the Lesser Antilles subduction zone using ocean-bottom seismometers (OBS) and reflection seismic equipment from Ifremer (Figure 3). The OBS recorded on three geophones and a hydrophone channel with a sampling rate of 4 ms (see Auffret et al. (2004) for technical description). Along profile AN06, 25 instruments were deployed at a regular spacing of 3 nautical miles (5.5 km). The reflection seismic equipment consisted of a 126 l (7699 cu. in.) tuned air-gun array and a full 2.8 km-long, 288 channel, digital seismic streamer.

Along wide-angle seismic line AN06, presented here, a total of 1180 high amplitude seismic shots were fired every 60 s and successfully recorded by the 25 OBS deployed on this profile. Many OBS recorded deep reflections from the subducting plate up to distances of 75 km resulting in excellent constraints on the deep velocity model (Figure 4). Pre-processing of the OBS data included calculation of the clock-drift corrections to adjust the clock in each instrument to the GPS base time. Instrument locations were corrected for the drift from the deployment position during their descent to the seafloor using the direct water wave arrival. Travel-time picking was performed on unfiltered data where possible to avoid timing errors due to the filtering. For low signal-to-noise ratios at longer offsets, a band-pass filter and deconvolution were used.

Among the phases used in this study are the main refracted p-wave arrivals from the oceanic crust, the forearc sediments and crust, and the upper mantle. Reflected arrivals were picked for all sedimentary and crustal layers. However, once the oceanic crust penetrates to depths greater than 20 km its geometry is mainly modeled from reflections from the top and bottom of that layer. Arrivals from the seismic reflection data were used to model the detailed layer geometry in the sediments. No s-wave arrivals were used in this study due to the poor quality of the arrivals.

The data processing sequence of the coincident MCS line includes band-pass filtering (2–7–60–80 Hz), FK filtering in order to reduce steep linear noise, external mutes to remove the direct and refracted waves, noise attenuation, internal mute, multiple modeling and attenuation, predictive deconvolution, iterative velocity analysis, normal and dip move-out corrections, and pre-stack time migration using a constant velocity (Boucard et al., 2021).

Bathymetric data were acquired using the Kongsberg-Simrad EM122 and Reson-Seabat 7150

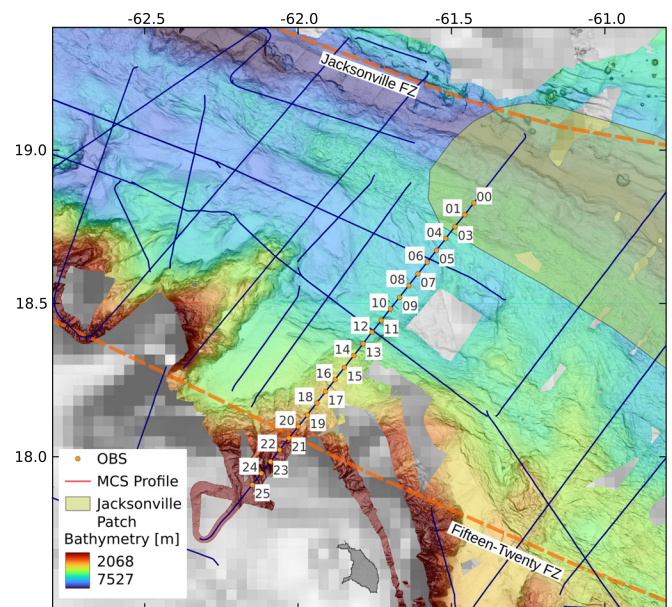


Figure 3 – Seafloor bathymetry recorded during cruises ANTITHESIS 1 and 3 with gaps in the coverage filled with data from satellite altimetry (Smith and Sandwell, 1997). The map shows the location of seismic lines (blue lines) and ocean bottom seismometers (yellow dots). Light green polygon depicts the Jacksonville Patch from Marcaillou et al. (2021).

dual multibeam system of *R/V L'Atalante* and *R/V Pourquoi pas?*, respectively, removing data outliers, gridded at a 100 m spacing and merged with bathymetric grids from earlier cruises (Deplus, 1998; Laigle et al., 2007; Patriat, 2007; Lebrun, 2009).

The wide-angle seismic data were modeled using a 2-D iterative damped least-squares travel-time inversion from the RAYINVR software (Zelt and Smith, 1992; Zelt, 1999). The model is defined by layers with depth and velocity nodes. Modeling was performed using a layer-stripping approach, proceeding from the top of the structure towards the bottom. In order to avoid smearing into the deeper layers of the model of the poorly constrained shallow model structure by the OBSs, upper layers were adjusted using a joint approach with the MCS reflection data. Arrival times of the main sedimentary layers and basement were picked from the seismic reflection data, converted to depth with streamer velocities, which were adjusted until calculated crustal reflection and refraction times fit with the travel-time picks. The depth and velocities of the crustal layers and the upper mantle were modeled from the OBS data only.

4 Results and error calculations

In the following we will present the wide-angle seismic model from forward modelling and estimations from different error calculations. We also present a gravity model which helps to constrain our model.

4.1 Wide-angle velocity model

The final velocity model shows the sedimentary and crustal structure down to a depth of 40 km for the

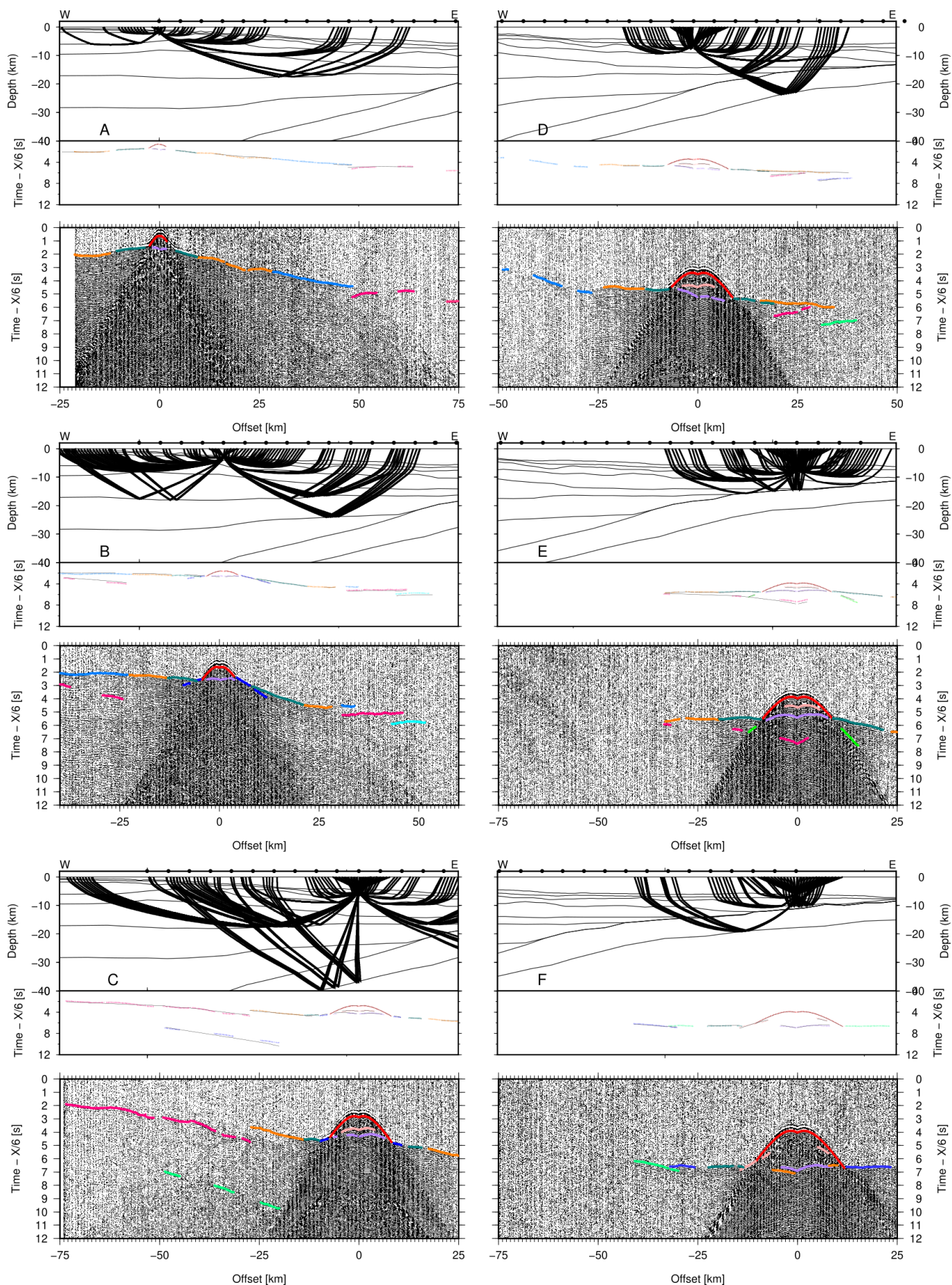


Figure 4 – Data, rayplots, picked and predicted arrival times for OBS 26 (A) OBS 22 (B) OBS 16 (C) OBS 13 (D) OBS06 (E) and OBS 00 (F). Only every 20th ray is shown and colors are explained in Table 1.

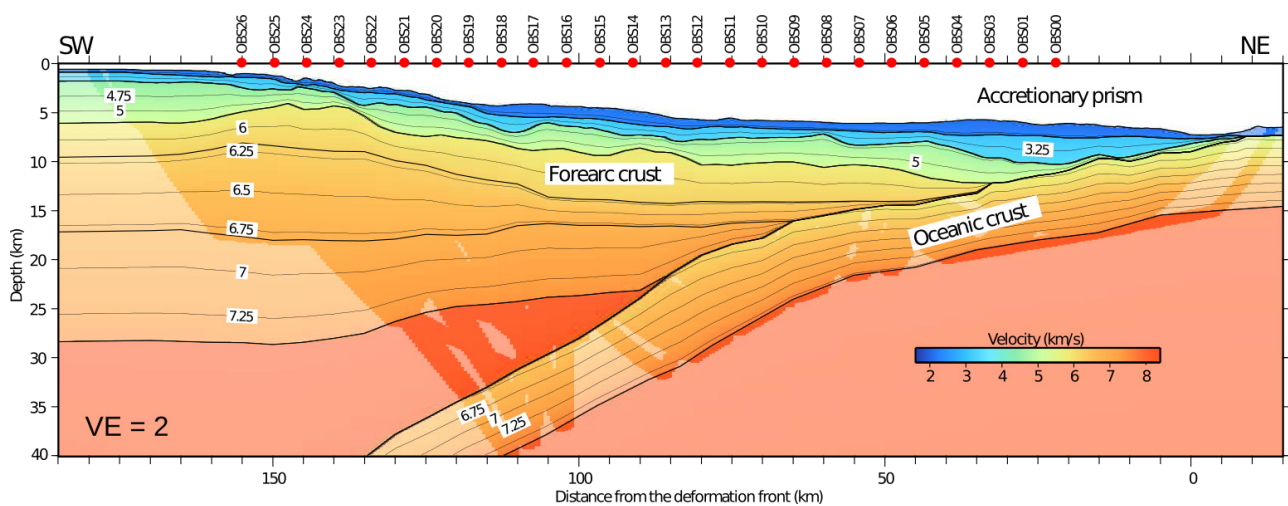


Figure 5 – Final velocity model from forward modeling. Velocity contours are shown every 0.25 km/s and ray coverage is indicated by increased color saturation. Red dots mark the locations of the seafloor instruments along the model.

lower plate and 26 km for the upper plate (Figure 5). The sedimentary cover thickens from several hundreds of meters on the oceanic crust to up to 5 km in the accretionary prism. It is modeled with one layer (velocities ranging from 2.1 up to 2.25 km/s) above the incoming oceanic plate and with two layers (velocities ranging from 2.1 up to 3.5 km/s) in the accretionary prism. The forearc crust is composed of four layers, with velocities of 4.5–5.5 km/s, 5.8–6.2 km/s, 6.2–6.8 km/s, and 6.9–7.4 km/s, respectively. The ~5.8 km thick subducting crust consists of one layer with velocities ranging from 5.2 to 7.7 km/s at shallow depth and from 6.2 to 7.8 km/s as it subducts into the deep mantle. The upper mantle velocities range between 8.2 km/s in the oceanic domain and 8.0–8.2 km/s in the mantle wedge. The resolution of the wide-angle seismic data at this depth does not allow us to constrain the thickness of the subduction channel. However, on a neighboring seismic reflection profile, a thickness ~0.2 to ~1 s twt has been proposed (Boucard *et al.*, 2021).

The fit between the final forward velocity model and the MCS profile is very good, as interfaces from the reflection section were included into the model. Lower velocities in the layers correspond to well stratified sedimentary units along the margin slope as well as poorly reflective and highly deformed sediments of the narrow accretionary prism (between model distance 0 to 25 km). Reflections from the top of the subducting crust are identifiable up to a model distance of 80 km on the MCS data and to 120 km on the WAS data (Figure 6).

4.2 Error estimation

We performed several different calculations to constrain the model resolution and depth uncertainty, as the accurate identification of velocity anomalies and the degree of resolution of the model fundamentally impact the conclusions of the work. To start with, the model parameterization is important for the quality of the resulting model (Figure 7a). The number of velocity and depth nodes should be adapted to the number of instruments used and the quality of the data. Including

a large amount of nodes into a model can lead to an over-fit of the data, with the creation of small anomalies which are not resolvable by the data but which minimize the model error. This would result in an unconstrained overall model. Since the geometry of the upper sedimentary layers is additionally constrained by the reflection seismic data, those shallow layers are not considered in the resolution tests detailed below. The fit between the predicted arrival times and the different picked travel-time phases is a first indicator of the model quality and all values are given in Table 1.

The point-spread function is calculated by perturbing a node and then inverting the perturbed model. If the model is poorly resolved for a given region, then one given node's perturbation will be smeared into adjacent nodes, possibly for both the velocities and the boundary depths, if both parameter types are involved. If the model region is well constrained the inversion will be identical or very close to the original model. Thus, the extent of the smearing indicates the spatial resolution of the model (Zelt, 1999). Perturbing single nodes allows for defining the spread-point function (SPF) giving the amount of smearing in different model regions (Figure 7b).

Two-point ray tracing between source and receiver for each picked phase (Figure 7c) shows the well resolved and the unconstrained areas. Ray coverage for diving and reflected waves is generally good due to the high data quality and close instrument spacing. All sedimentary layers are well sampled by reflected and turning rays in the model. The upper and middle crustal layers for the forearc upper plate are better sampled than the forearc lower crust, the lower plate's oceanic crust, and the mantle wedge in between. The lower plate's oceanic Moho at depth, the Caribbean plate's Moho, and the mantle wedge geometry are mainly constrained by reflected arrivals. The latter generally produces higher-amplitude arrivals than diving waves from layers of low seismic velocity gradients such as the upper mantle.

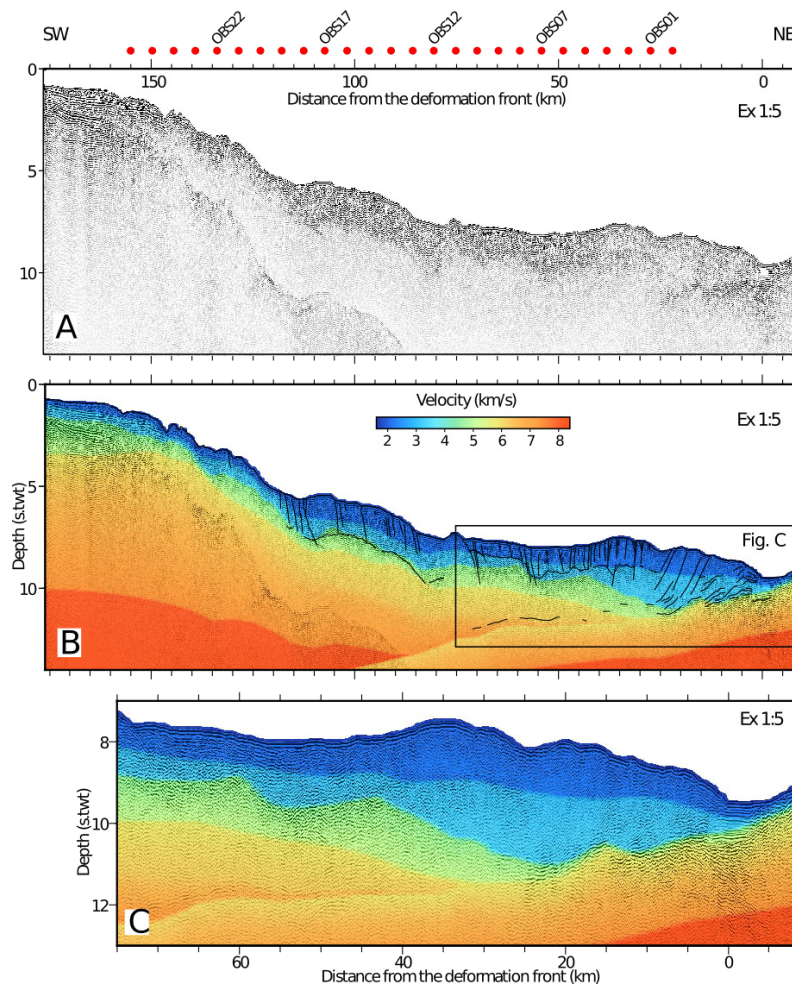


Figure 6 – (A) Reflection seismic profile AN06, coincident with the wide-angle seismic model. (B) Complete line underlain by the wide-angle seismic velocities : the black box shows the extent of the inset. (C) Zoom of the accretionary wedge and the downgoing slab.

The quality of the velocities and depth in the model can be estimated from the resolution parameter (see Figure 7d). Resolution is a measure of the number of rays passing through a region of the model constrained by a particular velocity node and is therefore dependent on the node spacing (Zelt, 1999). If a layer can be modeled with one single velocity gradient, the resolution parameter will be high even in areas which have lower ray coverage, as the area is related to only one velocity node. Nodes with values greater than 0.5 are considered as being well resolved (Figure 7d). The velocities for the sedimentary layers, the incoming plate, and the upper crust are well resolved. In contrast, fewer rays passing through deeper crustal layers and the upper mantle results in lower resolution.

4.3 Monte Carlo inversion

While forward models can take into account secondary reflections and information from coincident reflection seismic data, a major drawback is that the model can be dependent on *a priori* information included by the interpreter. Monte Carlo methods produce a large quantity of random models and test if any of those present a better or equal fit to the data. They have the advantage of being less biased by the interpreter's preferences than other error estimation methods and

give valuable insights into the uncertainties within the forward model. However, some parameters are generally not varied by Monte Carlo methods such as the number of layers.

We used the “Vmontecarlo” (Loureiro *et al.*, 2016) software to produce 50,000 independent random models, of which those that fit the threshold parameters (explain at least 95% of the picks of the preferred model and having an RMS error not higher than twice that of the preferred model) were selected for an uncertainty analysis (Loureiro *et al.*, 2016). All velocity nodes and the depth nodes of the crustal layers were tested, while the sedimentary depth layers, being additionally constrained by the reflection seismic data, were omitted. Moreover, nodes close to layer pinchouts were not analyzed since those can potentially produce a high number of random models characterized by unrealistic crossing layers. The resulting uncertainty sections show low uncertainties not exceeding 0.6 km/s in the crustal layers (Figure 8). The high uncertainties along Moho interfaces are due to velocity-depth trade off along the layer boundary (Loureiro *et al.*, 2016). There, different models may have the same interface at different depths and thus, the same cell can have velocities sampled from the layer above or below (Loureiro *et al.*, 2016). The thickness of this uncertainty zone shows the possible

Table 1 – Phase number, description, number of travel-time picks and RMS error for all phases and the complete model. The picking error was a constant 100 ms.

Phase #	Phase Name	Color in Figure 4	Number of Picks	RMS error
1	Water (direct phase)	■	2163	0.020
2	Sediment 1, turning phase	■	256	0.133
3	Sediment 1, reflection	■	234	0.124
4	Sediment 2, turning phase	■	966	0.094
5	Sediment 2, reflection	■	970	0.096
6	Arc basement, turning phase	■	1965	0.110
7	Arc Moho, reflection	■	343	0.225
8	Upper mantle, turning phase	■	56	0.405
9	Arc upper crust, turning phase	■	2378	0.079
11	Arc middle crust, turning phase	■	387	0.203
12	Arc intercrustal reflection	■	1900	0.196
13	Top subducting oceanic crust, reflection	■	71	0.268
14	Subducting oceanic crust, turning phase	■	583	0.189
15	Subducting oceanic Moho, reflection	■	479	0.125
17	Top subducting oceanic crust, reflection	■	171	0.098
Total			12922	0.129

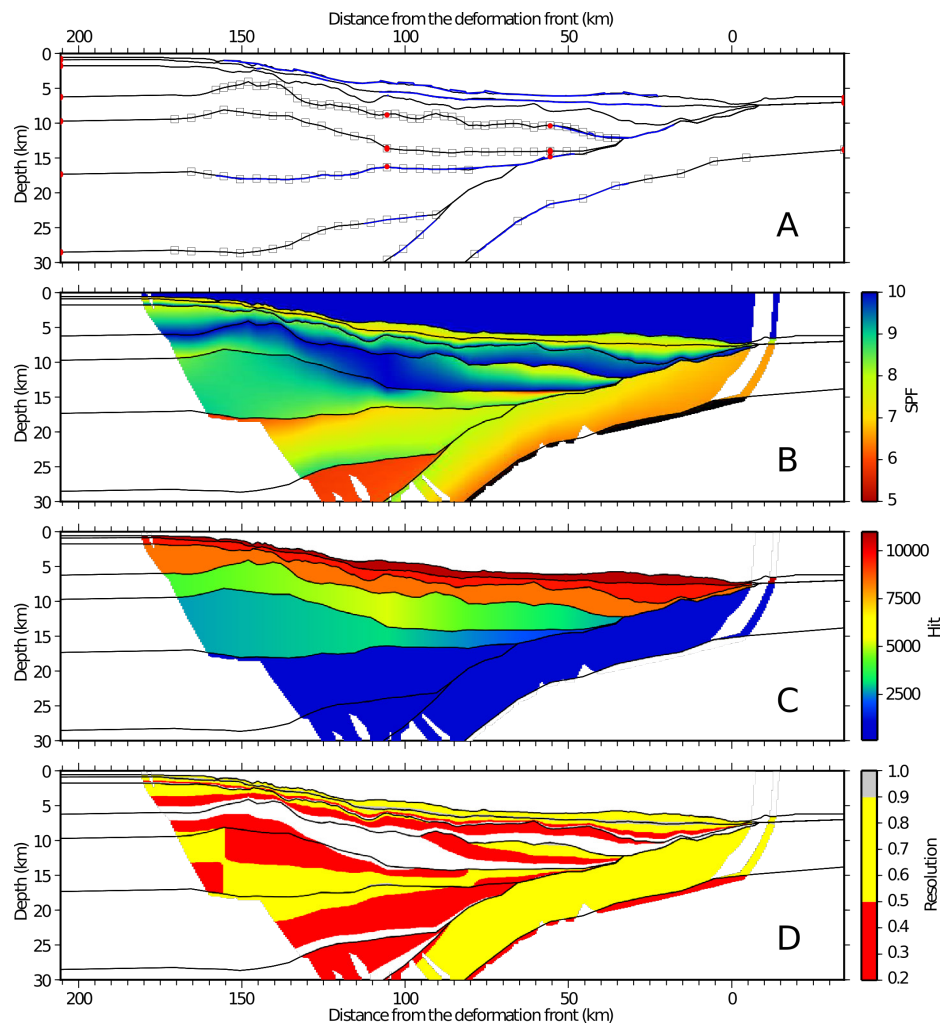


Figure 7 – Error estimate for the velocity model. (A) Model parameterization including interface depth nodes (squares), top and bottom layer velocity nodes (red circles) for the crustal layers. Interfaces constrained by reflections are highlighted in blue. (B) Smearing from the SPF for velocity (gridded and colored). (C) Ray hit count of velocity (gridded and colored) and depth nodes. (D) Resolution of velocity (gridded and colored) and depth nodes. Zones that are not imaged by wide-angle seismic data are shown in white.

depth range which is within a 1-km-thick band. The layer boundaries of the models showing the smallest error (dashed lines) are following closely the model boundaries of the preferred model. However, they show a greater

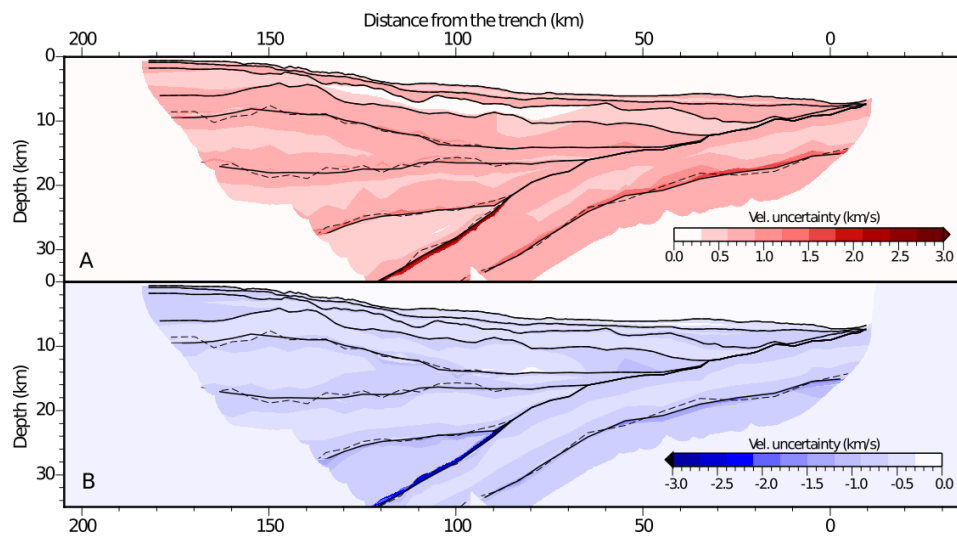


Figure 8 – Uncertainty plot of Profile 3 from Monte Carlo modeling. **(A)** Maximum and **(B)** minimum admissible velocity deviations from the preferred model, built from 50,000 models capable of tracing at least 12,276 rays (95% of the preferred models), with an RMS value under 195 ms (150% of the preferred models) and a χ^2 not exceeding 2.7 (150% of the preferred models). Shaded areas indicate ray coverage. Preferred model's interfaces are indicated with black lines. The best random model's interfaces are indicated with dashed lines.

variability which might imply that small artifacts are being fit, which we avoided by following the minimum structure approach. Concerning the mantle wedge, models with a thicker upper plate crust and a Moho depth greater than 30 km may explain the data equally well.

4.4 Gravity modeling

Since seismic velocities and rock densities are well correlated, gravity modeling allows us to confirm the large scale structures of the velocity model and extend this model into regions unconstrained by the seismic rays (Ludwig et al., 1970; Hamilton, 1978; Christensen and Mooney, 1995). Moreover, gravity modeling allows for detecting zones of anomalous density, like salt domes or regions of serpentinized mantle material. We used the “Gravmod” software from Colin Zelt to calculate a gravity anomaly predicted from our wide-angle seismic model (Zelt and Smith, 1992). To avoid edge effects, the model was extended by 100 km at both ends and down to a depth of 100 km.

The wide-angle seismic velocity model was converted layer by layer using the relationship $\rho = -0.6997 + 2.2302 V_p - 0.598 V_p^2 + 0.07036 V_p^3 - 0.0028311 V_p^4$, with ρ being the density and using a mantle density of a uniform 3.32 g/cm^3 . This is a fourth-order polynomial fit (C. A. Zelt, Gravmod user manual) to the relationship of Ludwig et al. (1970) (Figure 9). A comparison of this relationship to different density-velocity relationships from laboratory measurements shows that it clearly falls into the range of measured values (Ludwig et al., 1970; Hamilton, 1978; Carlson and Herrick, 1990; Hughes et al., 1998). We used the free-air anomaly from the WGM2012 (Bie et al., 2022b). Although density modeling is non-unique, comparing the anomaly predicted from the model to measured data can support the wide-angle seismic model and provide information about the lithology of deeper layers.

One factor which might alter densities of rocks is serpentinization, which is especially important in the marine environment. At slow spreading ridges, a high amount of mantle material is incorporated into the newly formed crust which then gets altered by seawater (Cannat et al., 2006; Smith, 2013). Faults from bending of the oceanic crust can create fluid paths that cross the crust and allow serpentinization of the upper mantle (Ranero et al., 2003). The compressional velocity varies with increasing degree of serpentinization where, for example, a 10-15% serpentinization of peridotites and dunites can reduce its density from 3.3 to 3.2 g/cm^3 (Christensen, 2004) (Figure 9).

Despite local mismatches in the oceanic domain, the predicted free-air gravity anomaly matches the satellite data resulting in a χ^2 -error of 31.9. To improve the fit of the model to the measured gravity anomaly, we used a slightly lower density simulating a serpentinization of the uppermost mantle of not more than 15% (Figure 10). In a second step the density of the incoming oceanic plate was reduced from 2.75 to 2.70 g/cm^3 , also simulating a reduced density of part of the crust due to serpentinized upper mantle material included into the crust at the mid-ocean ridge (Figure 10). These two changes from the original velocity-density relationship improve the fit to a χ^2 -error of 9.3. Measurements in serpentinites show a density variation between 3.3 g/cm^3 at 0% serpentinization to 2.4 g/cm^3 at 100% serpentinization at 1000 MPa and 400°C (Carlson and Müller, 2003; Carlson, 2003; Christensen, 2004) (Figure 9). Mixing highly serpentinized mantle material with gabbros or basalt might therefore lower the bulk density of the layer. The modeled density change would correspond to an increase of 10-20% of serpentinisation, but will not account for density or temperature effects. Dehydration starts at 40 km depth, as has been proposed based on numerical modelling (Rüpke et al., 2004).

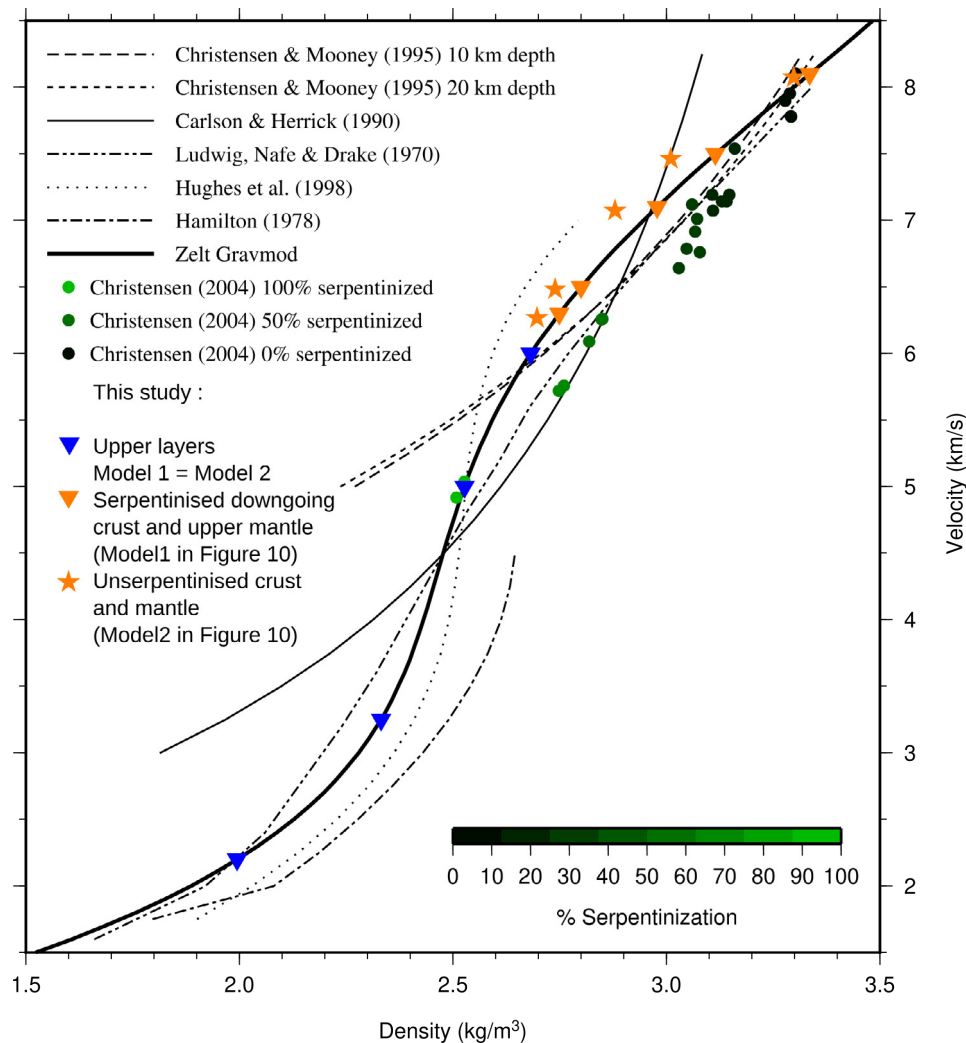


Figure 9 – Relationship between velocity and density from *Christensen and Mooney* (1995) for continental crust, *Ludwig et al.* (1970); *Hamilton* (1978); *Carlson and Herrick* (1990); *Hughes et al.* (1998) for marine environments. Light to dark green circles are data from laboratory experiments for peridotites serpentinized to different degrees (*Christensen*, 2004). The triangles and stars correspond to Model 1 (stars) and Model 2 (triangles) in Figure 10. The upper layers which are not changed are marked by blue inverted triangles and lower layers marked by orange triangles correspond to Model 1 without serpentinisation. The orange stars then reflect the decrease of density due to serpentinisation in Model 2.

5 Discussion

The comparison of the velocity model to other wide-angle seismic models allows for the investigation of along arc variations of the structure and velocities of the arc and the downgoing oceanic crust.

5.1 Variation of the nature of the downgoing oceanic crust

The existing TRAIL P2 profile is located 250 km to the South of AN06 profile, near the island of Guadeloupe (Figure 11). The slab dip is similar on both lines, although, locally at 70–80 km from the trench, a kink in the slab in line AN06 differs from the progressively increasing dip angle in the TRAIL P2 profile. In contrast, velocity-depth (V_z) profiles extracted below the basement at the oceanic crust show significant differences between these two lines. The slab crust is ~8-km-thick along the TRAIL P2 line and 5.8–6.5 km thick along line AN06, where lower crustal velocities are about 0.2 km/s higher. Moreover, the slab was successfully

modeled using a two layer model along the TRAIL P2 profile including a small but not well resolved (< 0.3 km/s) velocity discontinuity between both layers, while a single layer with constant velocity gradient along line AN06 provided the best fit to the data (Figure 10 and Figure 11).

We compare V_z -profiles on oceanic crust from both profiles with those for typical Atlantic and Pacific oceanic crust (*White et al.*, 1992) (blue polygons in Figure 11c) and those for regions of upper mantle material exhumed during early opening of oceanic basins (*Dean et al.*, 2000; *Van Avendonk et al.*, 2006) (green polygons in Figure 11d). Thickness and velocities in the AN06 model fit better to the outline of an upper mantle layer exhumed at the ocean floor, while the TRAIL P2 profile shows a better agreement with the outline of normal magmatic oceanic crust. These comparisons of the subducting slab with oceanic crust and exhumed upper mantle material suggest that the crust along the AN06 profile consists of material of a tectonically formed oceanic crust under magma-poor

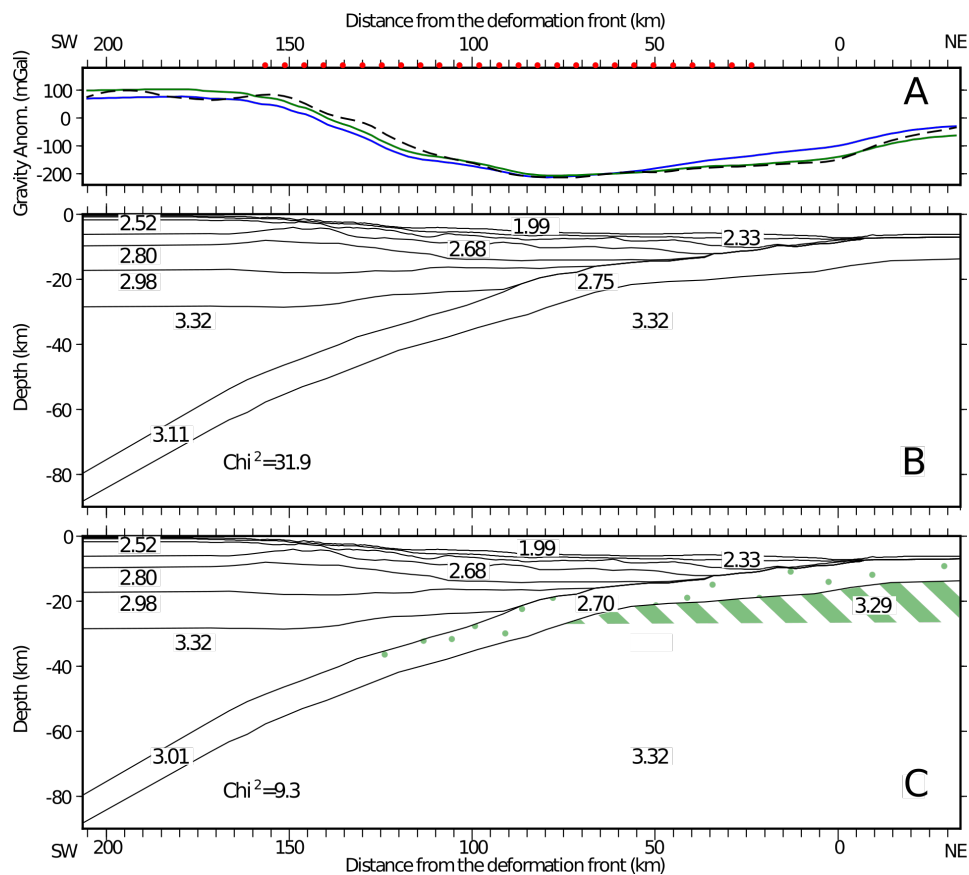


Figure 10 – Results of the gravity modeling. **(A)** Gravity anomaly from satellite altimetry (black dashed line) and predicted anomaly from the original velocity model 1 (blue line) and from model 2 including serpentinized upper mantle and oceanic crust (green line). Red dots show the OBS locations along the profile. **(B)** Density model from conversion of the velocity model. Black lines are the layer boundaries from the final velocity model. Densities are given by numbers in g/cm³. **(C)** Density model including serpentinized upper mantle and oceanic crust (green patterns) with black lines and numbers as in **(A)**.

spreading conditions, while a more magmatic oceanic crust may be imaged along the TRAIL P2 profile. This is consistent with the highly variable composition of oceanic crust produced at slow spreading ridges such as the Mid-Atlantic Ridge or the Southwest Indian Ridge, which might include large bodies of exhumed upper mantle material (Cannat, 1993; Escartín et al., 2008; Sauter et al., 2013). Moreover, variable oceanic crust was imaged along a N-S profile between the Barracuda Ridge (Fifteen-Twenty FZ) and the Mercurius FZ off the central Lesser Antilles trench (at longitude of 55°W), including three tectonically (i.e. partly hydrated crust) and two magmatically robust segments (i.e. mantle covered by two units of mafic crustal layering) (Figure 5 in Davy et al., 2020). Allen et al. (2019) similarly imaged on a profile located south of Barracuda Ridge and crossing the trench a tectonically accreted lithosphere entering into subduction. Comparing the results from our study to those of Davy et al. (2020) shows that while the velocities and thickness of the crust along the TRAIL P2 are comparable to segment centers in their study, the characteristics of oceanic crust along the AN06 profile better fit the segment's ends and fracture zone regions. This is in good agreement with our proposition that crust at the AN06 profile originates mainly from tectonic accretion.

In the MCS data, strong ridgeward dipping reflectors are imaged, which are deeply rooted (Figure 2). Furthermore, the Moho reflection is absent. This was interpreted as a patch (subsequently named the Jacksonville Patch) of serpentinized mantle rocks in the oceanic plate (Marcaillou et al., 2021). The authors suggested that this fabric was created at the Mid-Atlantic Ridge and then was reactivated by plate bending when the plate entered the subduction zone (Marcaillou et al., 2021). Heat-flow variations measured in the trench and the forearc during the ANTITHESIS cruise along the AN06 profile reveal heat-flow anomalies, negative in the trench and positive in the forearc, which indicate the existence of a ventilated fluid circulation with downward percolation of cold fluids at the sediment-starved trench and upward discharge of warm fluids through the forearc (Ezenwaka et al., 2022). From the wide-angle seismic data, the ridgeward dipping reflectors and the heat-flow anomalies lead us to suggest that the nature of the subducting oceanic crust is amagmatic, mostly built from exhumed and serpentinized upper mantle material bearing a high percentage of water. The AN06 WAS profile shows that the Jacksonville Patch extends at depth beneath the forearc crust. This suggests that all the plate interface crustal layer is underlain by highly hydrated and serpentinized crust. The peculiar nature of the downgoing plate might enrich the fluid circulation along

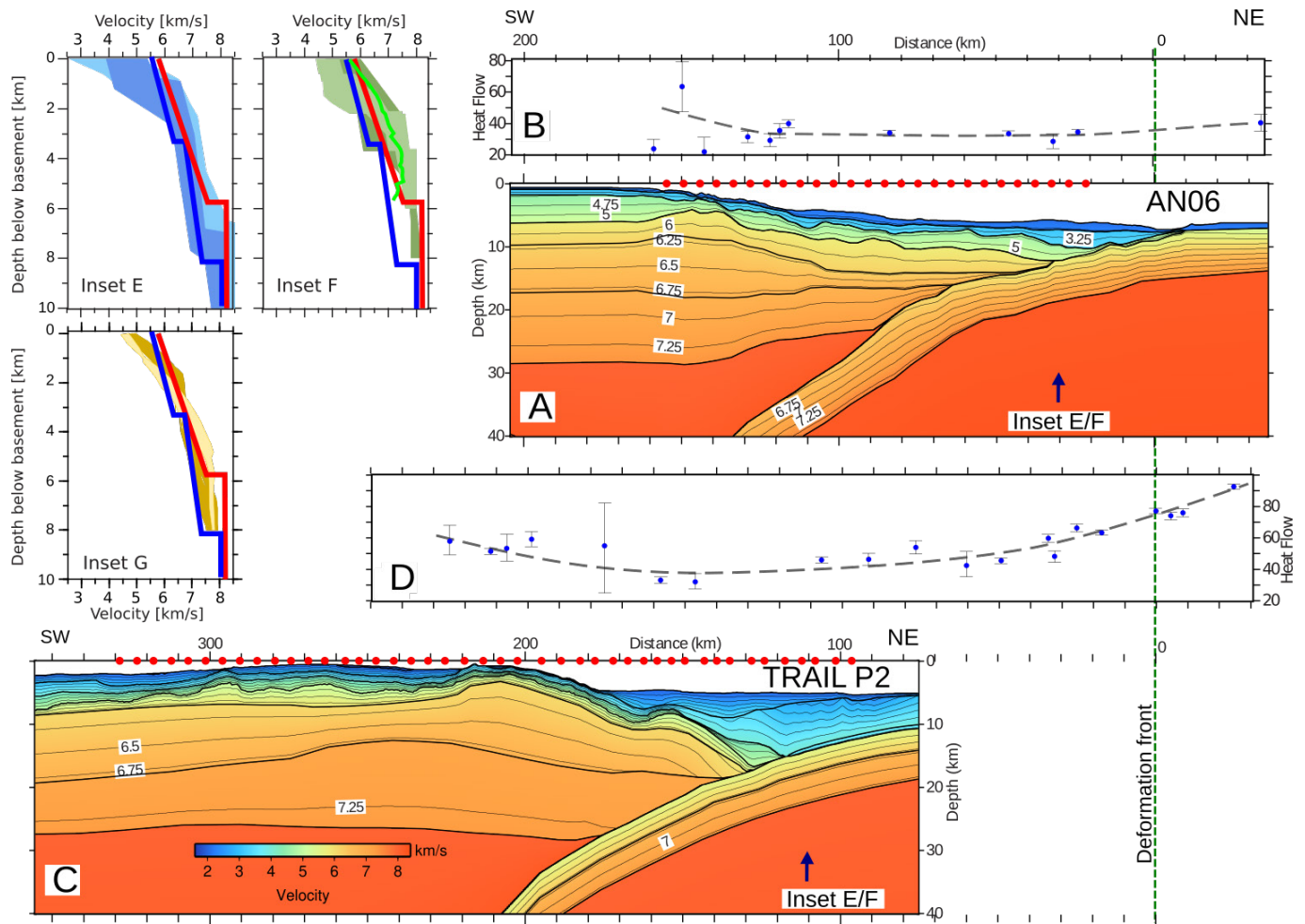


Figure 11 – (A) and (C) Wide-angle seismic models for line AN06 and the TRAIL P2 profile (Kopp et al., 2011), respectively, contoured at a 0.25 km/s interval. The position of the deformation front is marked by a green dashed line. The blue arrows correspond to the position of the vz-profiles shown in the insets (E), (F), and (G). (B) and (D) Heat flow values from Ezenwaka et al. (2022). For location see Figure 1. Insets: velocity-depth (vz) profiles extracted beneath the basement for the ANTITHESIS (red lines) and TRAIL P2 (blue lines) profiles. (E) Vz-profiles extracted from the oceanic crust region and comparison to typical Atlantic (144-170 Ma) and Pacific (29-140 Ma) crust (blue polygons - White et al., 1992). (F) Vz-profiles extracted from the oceanic crust region and comparison to velocities of exhumed upper mantle (light green polygon - Dean et al., 2000, dark green polygon - Van Avendonk et al., 2006). The green line marks the velocity distribution from tomographic inversion of first arrivals. The complete model is shown in electronic supplement S1. (G) Comparison to segment centers and segment ends from Davy et al. (2020).

the plate interface and through the margin from its dehydration between 40 and 70 km depth (Rüpke et al., 2004; Ezenwaka et al., 2022). Intense fluid circulation and the particular rheology of the serpentinite may favor sediment mobilization leading to the observed mud volcanism. The upward fluid migration may cause slope sediment destabilization and creeping at fault scarps and form mud-volcanoes at the toe of the fractured outer forearc margin. Furthermore, the rheology and fluid circulation may lower the fault rupture limit favoring creeping and slow slip seismic events that might be the cause of the reduced seismicity in the Jacksonville Patch region (Marcaillou et al., 2021) (Figure 2).

Moreover, heat-flow values at the trench along line AN06 (35-40 mW.m⁻²) are ~40% lower than along the TRAIL P2 profile (65-75mW.m⁻²) (Figure 11), and values in the trench of the Central and Southern Antilles (70-80 mW.m⁻²) (Ezenwaka et al., 2022). These heat-flow values are also significantly lower than

the expected 60-70 mW.m⁻² for 80 Myr old oceanic subducting plate (Stein and Stein, 1992). This low heat flow may be due to a depressed thermal structure of the oceanic crust related to the slow-spreading at the Mid-Atlantic Ridge. Low surface heat flow usually corresponds to cold temperatures along the interplate contact (Hyndman and Wang, 1993) and might influence the seismicity of the region. During the cruise we acquired bathymetric data from the oceanic crust to image the variation of its nature and morphology along the trench (Figure 12). While in the north round edifices can be identified, in the south undisturbed sediments are covering the plate. These edifices were created before the plate entered the subduction and its associated forebulge, and therefore might be associated to the nature of the accreted crust at the spreading center. Recent models of spreading mechanisms of slow spreading ridges propose the creation of core complexes and ridges close to the axis (Smith et al., 2006, 2008). These have a high serpentinite content and bring fluids

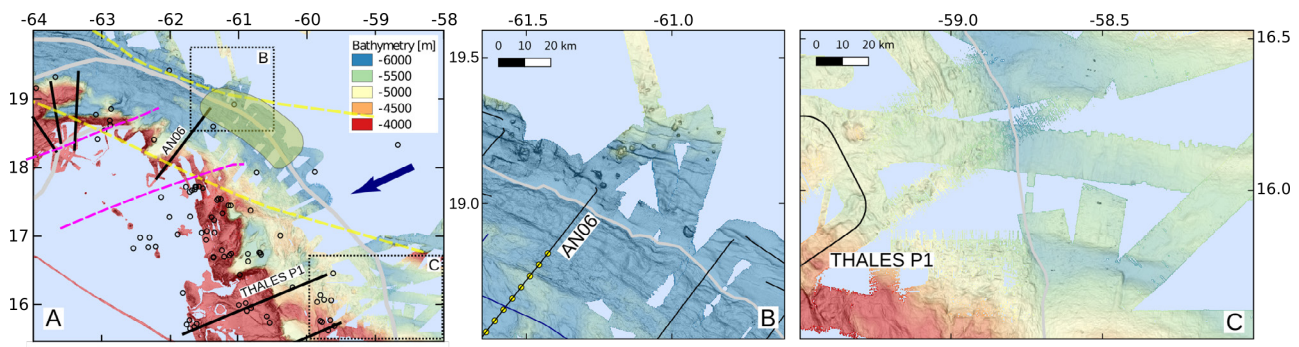


Figure 12 – (A) Seafloor bathymetry in the study region and position of the seismic lines. Jackson Patch is outlined by a yellow transparent patch, region of subducted seismicity is bound by violet dashed lines, and seismicity from the ISC catalogue by open black circles. (B) Seafloor bathymetry of the incoming oceanic plate in the region of the AN06 profile. (C) Seafloor bathymetry of the incoming oceanic plate in the region of the TRAIL P2 profile.

into the subduction zone. The serpentinite and the fluids might then interact with seismicity during subduction.

The difference in velocities in the downgoing slab between the TRAIL P2 and AN06 lines suggests that in the north the slab transports a higher fluid content, which is progressively expelled at depth and migrates back through the margin. As serpentinite rheology differs from that of basalt and gabbro and because the amount of fluid from dewatering serpentinite is significantly higher than from a mafic crust, the mechanical and rheological properties of the plate interface and the margin are likely to influence the interseismic coupling and slip behavior. The higher fluid content of the northern LASZ might directly influence the seismicity of the subduction zone. Indeed, if the hydrated state of the oceanic crust of the Jacksonville Patch originates from the Mid-Atlantic Ridge, and we extend the Jacksonville Patch in the direction of the subduction, a low seismicity corridor can be identified in seismological data (Figure 12) (Marcaillou et al., 2021). It has been proposed that this crust with high water content can impede large interplate earthquakes, and favor alternate slip behavior (for example, slow slip and tremor) (Schlaphorst et al., 2016; Paulatto et al., 2017; Marcaillou et al., 2021). However, both profiles in this comparison do not reach far onto oceanic crust, which might show a high variability, and the precision of the wide-angle seismic data below 15–20 km is naturally less accurate than in the region where oceanic crust is at shallower depths. These two points might hinder the precise constraining of the size of the Jacksonville Patch along our profile, but the additional constraints from other datasets clearly show the difference in the nature between the two regions. Tomographic inversion of the first arrivals along the AN06 profile reveals a very similar velocity distribution to that of the forward model (Figure 11 and electronic supplement S1).

5.2 Along arc variability of the structure of the Northern Lesser Antilles forearc crust

WAS profiles AN1–3–5 (Laurencin et al., 2018), AN06 (this study), GA03 (Padron et al., 2021), and TRAIL P2 (Kopp et al., 2011) provide crustal cross sections all along

the northern Lesser Antilles (Figure 1). Only the AN01 and AN06 profiles reach the trench, but all cover the outer slope of the margin down to the accretionary prism except the GA03 profile that ends in the outer forearc of La Désirade Basin (Figure 13). AN1–3–5–6 reach from the transition between the remnant volcanic arc and forearc domain out towards oceanic crust, whereas GA03 and THALES P1 span from the backarc domain and cross the remnant and present active volcanic arcs. A remarkable feature is the similarity in the structure between these profiles (Figure 13).

Overall, the forearc crust of the northern Lesser Antilles, i.e. from the Karukera Spur in the south to the Sombrero Basin in the north, only shows limited variability in thickness, between 22–27 km. This remains in the range of what previous studies observed beneath the Lesser Antilles volcanic arc which varies $30 \text{ km} \pm 5 \text{ km}$ (Arnaiz-Rodríguez et al., 2016; Gonzalez et al., 2018; Schlaphorst et al., 2018; Melekhova et al., 2019).

For comparison, the igneous part of the upper crustal level crops out and was sampled at the 4500 m high La Désirade scarp and at La Désirade Island. It consists of Late Jurassic – Early Cretaceous MORB-like and felsic rocks with a variable amount of arc signature (Neill et al., 2010). This illustrates that the forearc crust of the Northern Lesser Antilles was an integrated part of the Great Arc of the Caribbean (GAC) which was built during the eastward subduction of the Farallon plate beneath the proto-Caribbean Ocean prior to the subduction inversion during the mid-Cretaceous (Pindell and Kennan, 2009; Boschman et al., 2014). Then the volcanism of the mid-Cretaceous to present day GAC, following the subduction of the proto-Caribbean/Atlantic lithosphere westward, has intruded and contributed to building the crust of the NLA arc. Part of the forearc crustal thickness of the northern part of the NLA might result from tectonic movements.

However, the structure of the NLA forearc crust does not vary significantly laterally along strike with consistently a typical 3 layered crust of only slightly varying velocities (Figure 13). The upper-most layer with velocities $< 5.5 \text{ km/s}$ and a strong gradient consists

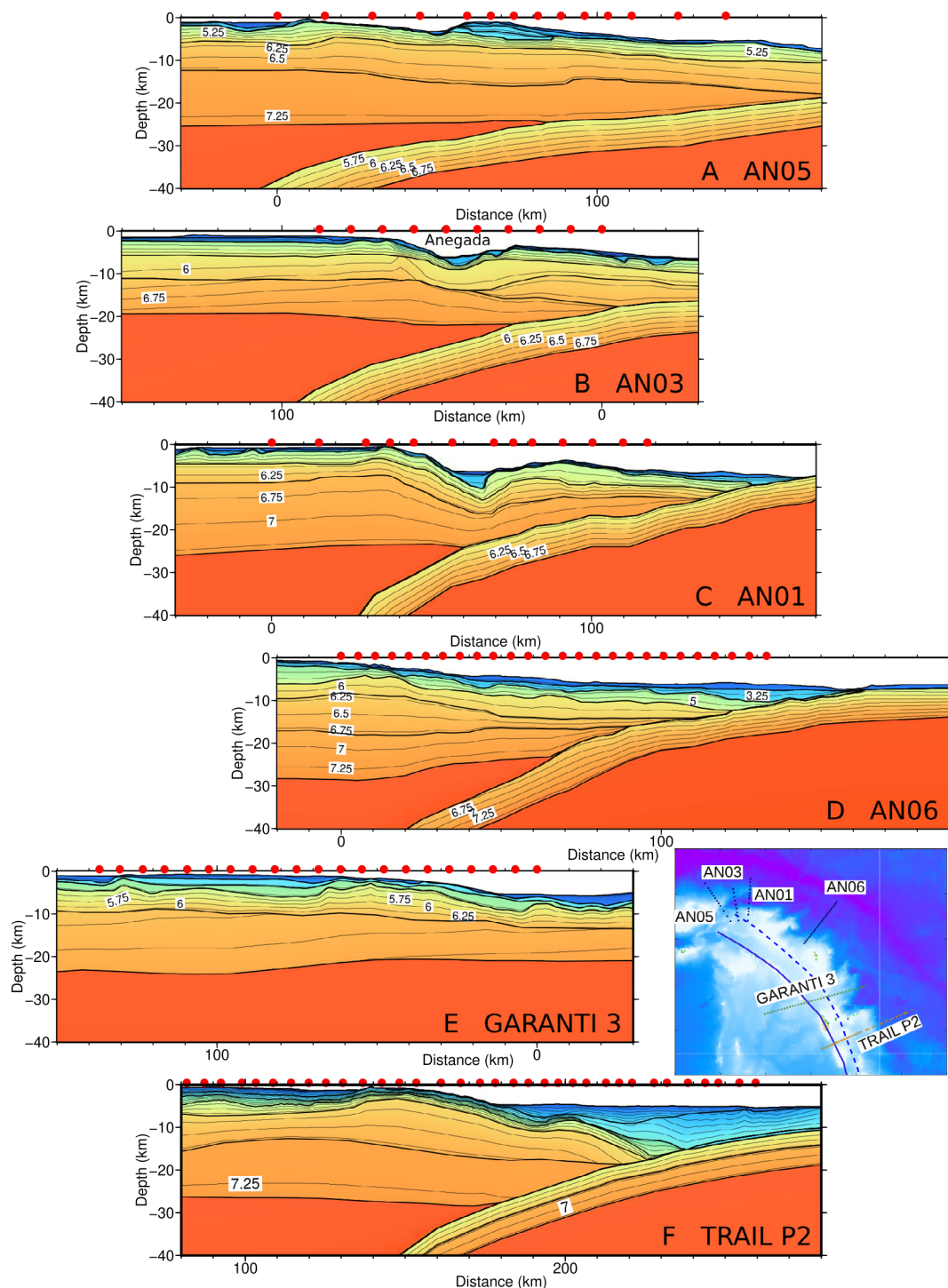


Figure 13 – Comparison of wide-angle seismic profiles along the Antilles Subduction zone (A, B, C) AN05, AN03, and AN01 profiles (Laurencin *et al.*, 2018) (D) AN06 (this study) (E) GARANTI 3 profile (Padron *et al.*, 2021) (F) TRAIL P2 profile (Kopp *et al.*, 2011). Inset shows line locations and the position of the modern and remnant Lesser Antilles volcanic arc (Bouysse, 1988).

of a variable thickness of sedimentary units and volcanoclastic or intrusive rocks probably fractured and partly altered. The mid-crustal layer presents velocities ranging from 5.5 to 6.8 km/s with a low gradient interpreted as a typical felsic arc crust. The lower crust unit with velocities between 6.8 and 7.3 km/s and low velocity gradients might consist of mafic plutons, similar to what has been proposed for the TRAIL P2 profile (Kopp *et al.*, 2011). Such layers can serve as a component for building continental crust through “foundering” or

delamination of the lower crustal layer (Kelemen *et al.*, 2003; Kopp *et al.*, 2011).

6 Conclusion

Compared to existing wide-angle seismic models in the Central Lesser Antilles, south of our study area, the new wide-angle seismic velocity model presented here clearly images for the first time a high velocity structure for the downgoing oceanic plate in the Lesser

Antilles. This velocity model suggests a composition affected by serpentinized ultramafic rocks typical of those identified at the present-day nearby Fifteen-Twenty fracture zone east of the trench (Davy *et al.*, 2020; Marcaillou *et al.*, 2021) and also at numerous locations along the slow-spreading Mid-Atlantic Ridge (Cannat *et al.*, 2006; Sauter *et al.*, 2013). Gravity modeling along the wide-angle seismic model is in good agreement with the velocity model if the lower plate and mantle density are significantly reduced to account for serpentinites within the subducting crust.

Variations in the seismicity of the Lesser Antilles might result from an interplay between the slab inclination decreasing to the north, local active faulting at crustal scale in the forearc domain in relation to the subduction of oceanic crustal highs, and the nature of the incoming slab, carrying highly variable water contents.

From WAS data acquired all along the Northern Lesser Antilles forearc, we show that the forearc crust presents little variation along the strike of the subduction zone and that it is similar in thickness and velocity structure to other arc crustal types rather than to thinned continental crust. The lower crustal unit velocities of the arc that reached 7.3 km/s probably result from arc mafic plutonic intrusions.

Acknowledgements

We thank the captain and crew of the *R/V Atalante* and *R/V Pourquoi Pas ?* for the data acquisition during the ANTITHESIS marine surveys (Marcaillou and Klingelhofer, 2013 - <https://doi.org/10.18142/242>). Many of the figures from this paper were drafted using the Generic Mapping Tools (<http://gmt.soest.hawaii.edu>) and the Seismic Unix software (<https://github.com/JohnWStockwellJr/SeisUnix/wiki>) (Cohen and Stockwell, 2003). The free OpendTect from dGB Earth Sciences (<https://www.dgbes.com/index.php/download>) and the open source QGIS software (<https://www.qgis.org/fr/site/forusers/download.html>) were used for data processing and drafting of several figures. We thank native speaking Marc-Andre Gutscher for help with language editing. We would like to thank two anonymous reviewers for their helpful and constructive comments.

Author contributions

The final forward modelling and error calculations were done by **FK**, **BM**, **LS** and **ML** undertook the processing and interpretation of the reflection seismic data. **JFL** and **ML** helped to put our model in the regional context. **HK** and **ME** helped with the comparison to the TRAIL and other lines from the Sismantilles experiment. All authors actively participated in writing and editing the text and figures.

Data availability

The ocean-bottom seismometer data used in this publication are accessible in standard SEG-Y format at the SEANOE data repository. The final wide-angle model and associated picks are freely available from the first author.

Competing interests

The authors declare no competing interests.

Peer review

This publication was peer-reviewed by two anonymous reviewers. The full peer-review report can be found here: [Review Report](#).

Copyright notice

© Author(s) 2025. This article is distributed under the Creative Commons Attribution 4.0 International License, which permits unrestricted use, distribution, and reproduction in any medium, provided the original author(s) and source are credited, and any changes made are indicated.

References

- Allen, R., J. Collier, A. Stewart, T. Henstock, S. Goes, and A. Rietbrock (2019), The role of arc migration in the development of the Lesser Antilles: A new tectonic model for the Cenozoic evolution of the eastern Caribbean, *Geology*, 47(9), 891–895, <https://doi.org/10.1130/G46708.1>.
- Arnaiz-Rodríguez, M. S., M. Schmitz, and F. Audemard (2016), Crustal structure of the Lesser Antilles arc estimated from receiver functions, *Revista Mexicana de Ciencias Geológicas*, 33(3), 286–296.
- Auffret, Y., P. Pelleau, F. Klingelhofer, L. Géli, J. Crozon, J. Lin, and J. Sibuet (2004), MicrOBS: A new generation of ocean bottom seismometer, *First Break*, 22(7), 41–47, <https://doi.org/10.3997/1365-2397.2004012>.
- Bangs, N. L., G. L. Christeson, and T. H. Shipley (2003), Structure of the Lesser Antilles subduction zone backstop and its role in a large accretionary system: LESSER ANTILLES SUBDUCTION ZONE BACKSTOP, *Journal of Geophysical Research*, 108(B7), <https://doi.org/10.1029/2002jb002040>.
- Barnes, P. M., L. M. Wallace, D. M. Saffer, R. E. Bell, M. B. Underwood, A. Fagereng, F. Meneghini, H. M. Savage, H. S. Rabinowitz, J. K. Morgan, H. Kitajima, S. Kutterolf, Y. Hashimoto, C. H. Engelmann de Oliveira, A. Noda, M. P. Crundwell, C. L. Shepherd, A. D. Woodhouse, R. N. Harris, M. Wang, S. Henrys, D. H. N. Barker, K. E. Petronotis, S. M. Bourlange, M. B. Clennell, A. E. Cook, B. E. Dugan, J. Elger, P. M. Fulton, D. Gamboa, A. Greve, S. Han, A. Hüpers, M. J. Ikari, Y. Ito, G. Y. Kim, H. Koge, H. Lee, X. Li, M. Luo, P. R. Malie, G. F. Moore, J. J. Mountjoy, D. D. McNamara, M. Paganoni, E. J. Screaton, U. Shankar, S. Shreedharan, E. A. Solomon, X. Wang, H.-Y. Wu, I. A. Pecher, L. J. LeVay, and IODP Expedition

- 372 Scientists (2020), Slow slip source characterized by lithological and geometric heterogeneity, *Science Advances*, 6(13), eaay3314, <https://doi.org/10.1126/sciadv.aay3314>.
- Bernard, P., and J. Lambert (1988), Subduction and seismic hazard in the northern Lesser Antilles: Revision of the historical seismicity, *Bulletin of the Seismological Society of America*, 78(6), 1965–1983, <https://doi.org/10.1785/BSSA0780061965>.
- Bie, L., A. Rietbrock, S. Hicks, R. Allen, J. Blundy, V. Clouard, J. Collier, J. Davidson, T. Garth, S. Goes, N. Harmon, T. Henstock, J. Hunen, M. Kendall, F. Krüger, L. Lynch, C. Macpherson, R. Robertson, K. Rychert, S. Tait, J. Wilkinson, and M. Wilson (2019), Along-arc heterogeneity in local seismicity across the Lesser Antilles subduction zone from a dense ocean-bottom seismometer network, *Seismological Research Letters*, 91(1), 237–247, <https://doi.org/10.1785/0220190147>.
- Bie, L., S. Hicks, A. Rietbrock, S. Goes, J. Collier, C. Rychert, N. Harmon, and B. Maunder (2022a), Imaging slab-transported fluids and their deep dehydration from seismic velocity tomography in the Lesser Antilles subduction zone, *Earth and Planetary Science Letters*, 586, 117,535, <https://doi.org/10.1016/j.epsl.2022.117535>.
- Bie, L., S. Hicks, A. Rietbrock, S. Goes, J. Collier, C. Rychert, N. Harmon, and B. Maunder (2022b), Imaging slab-transported fluids and their deep dehydration from seismic velocity tomography in the Lesser Antilles subduction zone, *Earth and Planetary Science Letters*, 586, 117,535, <https://doi.org/https://doi.org/10.1016/j.epsl.2022.117535>.
- Boschman, L. M., D. J. J. van Hinsbergen, T. H. Torsvik, W. Spakman, and J. L. Pindell (2014), Kinematic reconstruction of the Caribbean region since the Early Jurassic, *Earth-Science Reviews*, 138, 102–136, <https://doi.org/10.1016/j.earscirev.2014.08.007>.
- Boucard, M., B. Marcaillou, J. Lebrun, M. Laurencin, F. Klingelhofer, M. Laigle, S. Lallemand, L. Schenini, D. Graindorge, J. Cornée, P. Münch, M. Philippon, and the ANTITHESIS and GARANTI Scientif (2021), Paleogene V-shaped basins and Neogene subsidence of the Northern Lesser Antilles forearc, *Tectonics*, 40(3), e2020TC006,524, <https://doi.org/10.1029/2020TC006524>.
- Bouysse, P. (1988), Opening of the Grenada back-arc basin and evolution of the Caribbean plate during the Mesozoic and early Paleogene, *Tectonophysics*, 149(1-2), 121–143, [https://doi.org/10.1016/0040-1951\(88\)90122-9](https://doi.org/10.1016/0040-1951(88)90122-9).
- Cannat, M. (1993), Emplacement of mantle rocks in the seafloor at mid-ocean ridges, *Journal of Geophysical Research*, 98(B3), 4163–4172, <https://doi.org/10.1029/92jb02221>.
- Cannat, M., D. Sauter, V. Mendel, E. Ruellan, K. Okino, J. Escartín, V. Combier, and M. Baala (2006), Modes of seafloor generation at a melt-poor ultraslow-spreading ridge, *Geology*, 34(7), 605–608, <https://doi.org/10.1130/G22486.1>.
- Carlson, R., and D. Miller (2003), Mantle wedge water contents estimated from seismic velocities in partially serpentinized peridotites, *Geophysical Research Letters*, 30(5), <https://doi.org/10.1029/2002GL016600>.
- Carlson, R. L. (2003), Bound water content of the lower oceanic crust estimated from modal analyses and seismic velocities of oceanic diabase and gabbro: BOUND WATER CONTENT OF THE LOWER OCEANIC CRUST, *Geophysical Research Letters*, 30(22), <https://doi.org/10.1029/2003gl018213>.
- Carlson, R. L., and C. N. Herrick (1990), Densities and porosities in the oceanic crust and their variations with depth and age, *Journal of Geophysical Research*, 95(B6), 9153, <https://doi.org/10.1029/jb095ib06p09153>.
- Christensen, N. (2004), Serpentinites, Peridotites, and Seismology, *International Geology Review*, 46(9), 795–816, <https://doi.org/10.2747/0020-6814.46.9.795>.
- Christensen, N. I., and W. D. Mooney (1995), Seismic velocity structure and composition of the continental crust: A global view, *Journal of Geophysical Research, Solid Earth*, 100(B6), 9761–9788, <https://doi.org/10.1029/95JB00259>.
- Christeson, G., N. Bangs, and T. Shipley (2003), Deep structure of an island arc backstop, Lesser Antilles subduction zone, *Journal of Geophysical Research, Solid Earth*, 108(B7), 2327, <https://doi.org/10.1029/2002JB002243>.
- Cloos, M., and R. L. Shreve (1996), Shear-zone thickness and the seismicity of Chilean- and Marianas-type subduction zones, *Geology*, 24, 107–110, [https://doi.org/10.1130/0091-7613\(1996\)024<0107:SZTATS>2.3.CO;2](https://doi.org/10.1130/0091-7613(1996)024<0107:SZTATS>2.3.CO;2).
- Cohen, J. K., and J. W. Stockwell (2003), Seismic Unix Release 37: a free package for seismic research and processing, *Center for Wave Phenomena, Colorado School of Mines*.
- Collot, J., B. Marcaillou, F. Sage, F. Michaud, W. Agudelo, P. Charvis, D. Graindorge, M. Gutscher, and G. Spence (2004), Are rupture zone limits of great subduction earthquakes controlled by upper plate structures? Evidence from multichannel seismic reflection data acquired across the northern Ecuador–southwest Colombia margin, *Journal of Geophysical Research*, 109, B11,103, <https://doi.org/10.1029/2004JB003060>.
- Davy, R., J. Collier, T. Henstock, A. Rietbrock, S. Goes, J. Blundy, N. Harmon, C. Rychert, C. Macpherson, J. van Hunen, M. Kendall, J. Wilkinson, J. Davidson, M. Wilson, G. Cooper, B. Maunder, L. Bie, S. Hicks, R. Allen, B. Chichester, S. Tait, R. Robertson, J. Latchman, F. Krüger, J. Collier, T. Henstock, R. Allen, S. Butcher, G. Castiello, C. Chen, C. Harkin, D. Posse, B. Roche, A. Bird, A. Clegg, B. Pitcairn, M. Weeks, H. Kirk, and E. Labahn (2020), Wide-angle seismic imaging of two modes of crustal accretion in mature Atlantic Ocean crust, *Journal of Geophysical Research, Solid Earth*, 125, e2019JB019,100, <https://doi.org/10.1029/2019JB019100>.
- Dean, S. M., T. A. Minshall, R. B. Whitmarsh, and K. E. Loudon (2000), Deep structure of the ocean-continent transition in the southern Iberia Abyssal Plain from seismic refraction profiles: The IAM-9 transect at 40° 20' N, *Journal of Geophysical Research, Solid Earth*, 105(B3), 5859–5885.
- DeMets, C., P. E. Jansma, G. S. Mattioli, T. H. Dixon, F. Farina, R. Bilham, E. Calais, and P. Mann (2000), GPS geodetic constraints on Caribbean-North America Plate

- Motion, *Geophysical Research Letters*, 27(3), 437–440, <https://doi.org/10.1029/1999gl005436>.
- Deplus, C. (1998), AGUADOMAR cruise, L'Atalante R/V, <https://doi.org/10.17600/98010120>.
- Escartín, J., D. K. Smith, J. Cann, H. Schouten, C. Langmuir, and S. Escrig (2008), Central role of detachment faults in accretion of slow-spreading oceanic lithosphere, *Nature*, 455(7214), 790–794, <https://doi.org/10.1038/nature07333>.
- Evain, M., A. Galve, P. Charvis, M. Laigle, H. Kopp, A. Bécel, W. Weinzierl, A. Hirn, E. Flueh, and J. Gallart (2013), Structure of the Lesser Antilles subduction forearc and backstop from 3D seismic refraction tomography, *Tectonophysics*, 603, 55–67, <https://doi.org/10.1016/J.TECTO.2011.09.021>.
- Ezenwaka, K., B. Marcaillou, M. Laigle, F. Klingelhoef, J. Lebrun, M. Paulatto, Y. Biari, F. Rolandone, F. Lucazeau, A. Heuret, T. Pichot, and H. Bouquerel (2022), Thermally-constrained fluid circulation and seismicity in the Lesser Antilles subduction zone, *Earth and Planetary Science Letters*, 597, 117,823, <https://doi.org/10.1016/j.epsl.2022.117823>.
- Feuillet, N., F. Beauducel, and P. Tapponnier (2011), Tectonic context of moderate to large historical earthquakes in the lesser Antilles and mechanical coupling with volcanoes, *Journal of Geophysical Research, Solid Earth*, 116(B10), 1–26, <https://doi.org/10.1029/2011JB008443>.
- Gonzalez, O., V. Clouard, S. Tait, and G. Panza (2018), S-wave velocities of the lithosphere-asthenosphere system in the Lesser Antilles from the joint inversion of surface wave dispersion and receiver function analysis, *Tectonophysics*, 734, 1–15, <https://doi.org/10.1016/J.TECTO.2018.03.021>.
- Hamilton, E. (1978), Sound velocity–density relations in sea-floor sediments and rocks, *The journal of the Acoustical Society of America*, 63, 366–377, <https://doi.org/10.1121/1.381747>.
- Harvard Geospatial Library (2003), Volcanoes of the world, <https://hgl.harvard.edu/catalog/harvard-glb-volc>.
- Hough, S. (2013), Missing great earthquakes, *Journal of Geophysical Research, Solid Earth*, 118(3), 1098–1108, <https://doi.org/10.1002/jgrb.50083>.
- Hughes, S., P. Barton, and D. Harrison (1998), Exploration in the Shetland-Faeroe Basin using densely spaced arrays of ocean-bottom seismometers, *Geophysics*, 63(2), 490–501, <https://doi.org/10.1190/1.1444350>.
- Hyndman, R., and K. Wang (1993), Thermal constraints on the zone of major thrust earthquake failure: The Cascadia Subduction Zone, *Journal of Geophysical Research*, 98, 2039–2060, <https://doi.org/10.1029/92JB02279>.
- International Seismological Centre (2022), ISC-GEM Earthquake Catalogue, <https://doi.org/10.31905/d808b825>.
- Jagoutz, O., and P. Kelemen (2015), Role of arc processes in the formation of continental crust, *Annual Review of Earth and Planetary Sciences*, 43, 363–404, <https://doi.org/10.1146/ANNUREV-EARTH-040809-152345>.
- Kay, R., and S. Kay (1993), Delamination and delamination magmatism, *Tectonophysics*, 219(1-3), 177–189, [https://doi.org/10.1016/0040-1951\(93\)90295-U](https://doi.org/10.1016/0040-1951(93)90295-U).
- Kelemen, P. B., K. Hanghøj, and A. R. Greene (2003), One view of the geochemistry of subduction-related magmatic arcs, with an emphasis on primitive andesite and lower crust, *Treatise on Geochemistry*, 3, 659.
- Kopp, H., W. Weinzierl, A. Becel, P. Charvis, M. Evain, E. R. Flueh, A. Gailler, A. Galve, A. Hirn, A. Kandilarov, D. Klaeschen, M. Laigle, C. Papenberg, L. Planert, and E. Roux (2011), Deep structure of the central Lesser Antilles Island Arc: Relevance for the formation of continental crust, *Earth and Planetary Science Letters*, 304(1-2), 121–134, <https://doi.org/10.1016/j.epsl.2011.01.024>.
- Laigle, M., J. F. Lebrun, and A. Hirn (2007), SISMANTILLES 2 cruise, L'Atalante R/V, <https://doi.org/10.17600/7010020>.
- Laigle, M., A. Hirn, M. Sapin, A. Bécel, P. Charvis, E. Flueh, J. Diaz, J. Lebrun, A. Gesret, R. Raffaele, A. Galve, M. Evain, M. Ruiz, H. Kopp, G. Bayrakci, W. Weinzierl, Y. Hello, J. Lépine, J. Viodé, M. Sachpazi, J. Gallart, E. Kissling, and R. Nicolich (2013a), Seismic structure and activity of the north-central Lesser Antilles subduction zone from an integrated approach: Similarities with the Tohoku forearc, *Tectonophysics*, 603, 1–20, <https://doi.org/10.1016/J.TECTO.2013.05.043>.
- Laigle, M., A. Becel, B. de Voogd, M. Sachpazi, G. Bayrakci, J.-F. Lebrun, and M. Evain (2013b), Along-arc segmentation and interaction of subducting ridges with the Lesser Antilles Subduction forearc crust revealed by MCS imaging, *Tectonophysics*, 603, 32–54, <https://doi.org/10.1016/j.tecto.2013.05.028>.
- Lardeaux, J., P. Münch, M. Corsini, J. Cornée, C. Vérati, J. Lebrun, F. Quillévéré, M. Melinte-Dobrinescu, J. Léticée, J. Fietzke, Y. Mazabraud, F. Cordey, and A. Randrianasolo (2013), La Désirade island (Guadeloupe, French West Indies): a key target for deciphering the role of reactivated tectonic structures in Lesser Antilles arc building, *Bulletin de la Société Géologique de France*, 184(1-2), 21–34, <https://doi.org/10.2113/GSSGFBULL.184.1-2.21>.
- Laurencin, M., D. Graindorge, F. Klingelhoef, B. Marcaillou, and M. Evain (2018), Influence of increasing convergence obliquity and shallow slab geometry onto tectonic deformation and seismogenic behavior along the Northern Lesser Antilles zone, *Earth and Planetary Science Letters*, 492, 59–72, <https://doi.org/10.1016/J.EPSL.2018.03.048>.
- Laurencin, M., B. Marcaillou, D. Graindorge, J.-F. Lebrun, F. Klingelhoef, M. Boucard, M. Laigle, S. Lallemand, and L. Schenini (2019), The Bunce Fault and strain partitioning in the Northern Lesser Antilles, *Geophysical Research Letters*, 46(16), 9573–9582, <https://doi.org/10.1029/2019gl083490>.
- Lebrun, J. F. (2009), KASHALLOW 2 cruise, Le Suroît R/V, <https://doi.org/10.17600/9020010>.

- Loureiro, A., A. Afilhado, L. Matias, M. Moulin, and D. Aslanian (2016), Monte Carlo approach to assess the uncertainty of wide-angle layered models: Application to the Santos Basin, Brazil, *Tectonophysics*, 683, 286–307, <https://doi.org/10.1016/J.TECTO.2016.05.040>.
- Ludwig, W. J., J. E. Nafe, and C. L. Drake (1970), *The Sea, Vol. 4, Part 1*.
- Marcaillou, B., and F. Klingelhofer (2013), ANTITHESIS LEG1 cruise, L'Atalante R/V, <https://doi.org/10.17600/13010070>.
- Marcaillou, B., F. Klingelhofer, M. Laurencin, J. Lebrun, M. Laigle, S. Lallemand, L. Schenini, A. Gay, M. Boucard, K. Ezenwaka, and D. Graindorge (2021), Pervasive detachment faults within the slow spreading oceanic crust at the poorly coupled Antilles subduction zone, *Communications Earth & Environment*, 2(1), 203, <https://doi.org/10.1038/s43247-021-00269-6>.
- Massin, F., V. Clouard, I. Vorobieva, F. Beauducel, J. Saurel, C. Satriano, M. Bouin, and D. Bertil (2021), Automatic picking and probabilistic location for earthquake assessment in the Lesser Antilles subduction zone (1972–2012), *Comptes Rendus: Geoscience*, 353(S1), 187–209, <https://doi.org/10.5802/crgeos.81>.
- Mccaffrey, R. (2008), Global frequency of magnitude 9 earthquakes, *Geology*, 36(3), 263–266, <https://doi.org/10.1130/G24402A.1>.
- Melekhova, E., D. Schlaphorst, J. Blundy, J. Kendall, C. Connolly, A. McCarthy, and R. Arculus (2019), Lateral variation in crustal structure along the Lesser Antilles arc from petrology of crustal xenoliths and seismic receiver functions, *Earth and Planetary Science Letters*, 516, 12–24, <https://doi.org/10.1016/J.EPSL.2019.03.030>.
- Neill, I., J. A. Gibbs, A. Hastie, and A. Kerr (2010), Origin of the volcanic complexes of La Désirade, Lesser Antilles: Implications for tectonic reconstruction of the Late Jurassic to Cretaceous Pacific-proto Caribbean margin, *Lithos*, 120(3–4), 407–420, <https://doi.org/10.1016/J.LITHOS.2010.08.026>.
- Nikolaeva, K., T. Gerya, and J. Connolly (2008), Numerical modelling of crustal growth in intraoceanic volcanic arcs, *Physics of the Earth and Planetary Interiors*, 171(1–4), 336–356, <https://doi.org/10.1016/J.PEPI.2008.06.026>.
- Padron, C., F. Klingelhofer, B. Marcaillou, J. F. Lebrun, S. Lallemand, C. Garroq, and G. C. Team (2021), Deep structure of the Grenada Basin from wide-angle seismic, bathymetric and gravity data, *Journal of Geophysical Research, Solid Earth*, 126(2), e2020JB020472.
- Patriat, M. (2007), ANTIPLAC cruise, L'Atalante R/V, <http://doi.org/10.17600/7010010>.
- Paulatto, M., M. Laigle, A. Galve, P. Charvis, M. Sapin, G. Bayrakci, M. Evain, and H. Kopp (2017), Dehydration of subducting slow-spread oceanic lithosphere in the Lesser Antilles, *Nature Communications*, 8, 15,980, <https://doi.org/10.1038/ncomms15980>.
- Pindell, J. L., and L. Kennan (2009), Tectonic evolution of the Gulf of Mexico, Caribbean and northern South America in the mantle reference frame: an update, *Geological Society Special Publication*, 328(1), 1–55, <https://doi.org/10.1144/sp328.1>.
- Ranero, C., J. Morgan, K. McIntosh, and C. Reichert (2003), Bending-related faulting and mantle serpentinization at the Middle America trench, *Nature*, 425, 367–373, <https://doi.org/10.1038/nature01961>.
- Ruff, L., and H. Kanamori (1980), Seismicity and the subduction process, *Physics of the Earth and Planetary Interiors*, 23(3), 240–252, [https://doi.org/10.1016/0031-9201\(80\)90117-X](https://doi.org/10.1016/0031-9201(80)90117-X).
- Rüpke, L., J. Morgan, M. Hort, and J. Connolly (2004), Serpentine and the subduction zone water cycle, *Earth and Planetary Science Letters*, 223(1–2), 17–34, <https://doi.org/10.1016/J.EPSL.2004.04.018>.
- Sauter, D., M. Cannat, S. Rouméjon, M. Andréani, D. Birot, A. Bronner, D. Brunelli, J. Carlut, A. Delacour, V. Guyader, C. MacLeod, G. Manatschal, V. Mendel, B. Ménez, V. Pasini, E. Ruellan, and R. Searle (2013), Continuous exhumation of mantle-derived rocks at the Southwest Indian Ridge for 11 million years, *Nature Geoscience*, 6(4), 314–320, <https://doi.org/10.1038/NGEO1771>.
- Schlaphorst, D., J. Kendall, J. Collier, J. Verdon, J. Blundy, B. Baptie, J. Latchman, F. Massin, and M. Bouin (2016), Water, oceanic fracture zones and the lubrication of subducting plate boundaries—insights from seismicity, *Geophysical Journal International*, 204(3), 1405–1420, <https://doi.org/10.1093/GJI/GGV509>.
- Schlaphorst, D., E. Melekhova, J. Kendall, J. Blundy, and J. Latchman (2018), Probing layered arc crust in the Lesser Antilles using receiver functions, *Royal Society Open Science*, 5(11), 180,764, <https://doi.org/10.1098/rsos.180764>.
- Scholz, C., and C. Small (1997), The effect of seamount subduction on seismic coupling, *Geology*, 25, 487–490, [https://doi.org/10.1130/0091-7613\(1997\)025<0487:TEOSSO>2.3.CO;2](https://doi.org/10.1130/0091-7613(1997)025<0487:TEOSSO>2.3.CO;2).
- Smith, D. K. (2013), Tectonics: Mantle spread across the sea floor, *Nature Geoscience*, 6, 247–248, <https://doi.org/10.1038/NGEO1786>.
- Smith, D. K., J. Cann, and J. Escartín (2006), Widespread active detachment faulting and core complex formation near 13 degrees N on the Mid-Atlantic Ridge, *Nature*, 442(7101), 440–443, <https://doi.org/10.1038/nature04950>.
- Smith, D. K., J. Escartín, H. Schouten, and J. Cann (2008), Fault rotation and core complex formation: Significant processes in seafloor formation at slow-spreading mid-ocean ridges (Mid-Atlantic Ridge, 13°–15°N), *Geochemistry, Geophysics, Geosystems*, 9(3), <https://doi.org/10.1029/2007GC001699>.
- Smith, W. H. F., and D. Sandwell (1997), Global sea floor topography from satellite altimetry and ship depth soundings, *Science*, 277(5334), 1956–1962, <https://doi.org/10.1126/SCIENCE.277.5334.1956>.
- Stein, C., and S. Stein (1992), A model for the global variation in oceanic depth and heat flow with lithospheric age, *Nature*, 359(6391), 123–129, <https://doi.org/10.1038/359123A0>.

- Symithe, S., E. Calais, J. D. Chabalier, R. Robertson, and M. Higgins (2015), Current block motions and strain accumulation on active faults in the Caribbean, *Journal of Geophysical Research, Solid Earth*, 120(5), 3748–3774, <https://doi.org/10.1002/2014JB011779>.
- Taylor, S. (1967), The origin and growth of continents, *Tectonophysics*, 4(1), 17–34, [https://doi.org/10.1016/0040-1951\(67\)90056-X](https://doi.org/10.1016/0040-1951(67)90056-X).
- Tsuru, T., J.-O. Park, S. Miura, S. Kodaira, Y. Kido, and T. Hayashi (2002), Along-arc structural variation of the plate boundary at the Japan Trench margin: Implication of interplate coupling, *Journal of Geophysical Research*, 107, 2357, <https://doi.org/10.1029/2001JB001664>.
- Van Avendonk, H. V., W. Holbrook, G. Nunes, D. Shillington, B. Tucholke, K. Loudon, H. Larsen, and J. Hopper (2006), Seismic velocity structure of the rifted margin of the eastern Grand Banks of Newfoundland, Canada, *Journal of Geophysical Research, Solid Earth*, 111(B11), <https://doi.org/10.1029/2005JB004156>.
- van Rijsingen, E., E. Calais, R. Jolivet, J. de Chabalier, J. Jara, S. Symithe, R. Robertson, and G. Ryan (2020), Inferring interseismic coupling along the Lesser Antilles arc: A Bayesian approach, *Journal of Geophysical Research, Solid Earth*, 126(2), e2020JB020677, <https://doi.org/10.1029/2020JB020677>.
- Wallace, L., A. Fagereng, and S. Ellis (2012), Upper plate tectonic stress state may influence interseismic coupling on subduction megathrusts, *Geology*, 40(10), 895–898, <https://doi.org/10.1130/G33373.1>.
- Wang, K., and S. Bilek (2011), Do subducting seamounts generate or stop large earthquakes, *Geology*, 39, 819–822, <https://doi.org/10.1130/G31856.1>.
- Westbrook, G., J. Ladd, P. Buhl, N. Bangs, and G. Tiley (1988), Cross section of an accretionary wedge: Barbados Ridge complex, *Geology*, 16(7), 631–635, [https://doi.org/10.1130/0091-7613\(1988\)016<0631:CSOAAW>2.3.CO;2](https://doi.org/10.1130/0091-7613(1988)016<0631:CSOAAW>2.3.CO;2).
- White, R., D. McKenzie, and R. O’Nions (1992), Oceanic crustal thickness from seismic measurements and rare earth element inversions, *Journal of Geophysical Research, Solid Earth*, 97(B13), 19,683–19,715, <https://doi.org/10.1029/92JB01749>.
- Zahibo, N., and E. N. Pelinovsky (2001), Evaluation of tsunami risk in the Lesser Antilles, *Natural Hazards and Earth System Sciences*, 1(4), 221–231, <https://doi.org/10.5194/nhess-1-221-2001>.
- Zelt, C. (1999), Modelling strategies and model assessment for wide-angle seismic traveltime data, *Geophysical Journal International*, 139(1), 183–204, <https://doi.org/10.1046/J.1365-246X.1999.00934.X>.
- Zelt, C., and R. B. Smith (1992), Seismic traveltime inversion for 2-D crustal velocity structure, *Geophysical Journal International*, 108(1), 16–34, <https://doi.org/10.1111/J.1365-246X.1992.TB00836.X>.